Reliability Engineering and System Safety 217 (2022) 108072

Contents lists available at ScienceDirect

Reliability Engineering and System Safety

journal homepage: www.elsevier.com/locate/ress

Framework for probabilistic simulation of power transmission network performance under hurricanes

Liyang Ma [a], Vasileios Christou [b], Paolo Bocchini [a,*]

[a] Department of Civil and Environmental Engineering, ATLSS Engineering Research Center, Lehigh University, 117 ATLSS Drive, Bethlehem, PA 18015-4729, USA
[b] Fermat Capital Management, LLC 615 Riverside Ave, Westport, CT 06880

ARTICLE INFO

Keywords:
Physics-based fragility models
Hurricane simulator
Transmission network
Random field
Power transmission system resilience
Wind direction

ABSTRACT

Structures in a power transmission network, such as towers and conductors, are vulnerable to hurricanes. Failures of these structures trip transmission lines and usually result in large scale power outages in the region. This paper presents a technique for the probabilistic simulation of power transmission systems under hurricane events and provides fundamental insights on the modeling and quantification of power system performance and resilience. The study models the power transmission system as a network of connected individual components, which are subjected to wind-induced mechanical failure and power flow constraints. A realistic power transmission network is developed for the study region. The geographical data are obtained for all components in the network based on a data collection and image processing campaign to reflect the realistic properties of the network serving the Lehigh Valley, PA. A hurricane simulator is utilized to generate a hurricane scenario providing time-varying wind intensities and wind directions for the component failure analysis. The spatio-temporal impact of the hurricane is investigated: a pool of component fragilities is generated to effectively incorporate the uncertainties in structural capacities into the analysis; the spatial correlation among structures is modeled efficiently by a random field based technique. At the system level, Monte Carlo simulation is adopted to determine the failure probability of transmission lines. The unmet demand of the system is computed probabilistically, based on the alternate current optimal power flow analysis, capacity constraints and load shedding process of the system. The simulation results can be used to quantify and visualize the power network performance, and help decision makers to identify critical components in the network to optimize the short-term pre-event preparation for an approaching hurricane and long-term retrofit strategy to enhance system resilience.

1. Introduction

Power transmission networks transport bulk power energy from power generation sites to power distribution sites over long distances, through high-voltage electrical conductors supported by transmission towers. It is one of the most critical infrastructure systems for the modern society, since the transportation, water and health care systems all depend on the supply of electrical energy. The interdependence between the power infrastructure and other infrastructures have been investigated and modeled by various researchers [1–3]. The power network is vulnerable to multiple types of natural and man-made hazards. For instance, the performance of power transmission networks under earthquake events was studied by Shinozuka et al. [4]. The overhead transmission lines are very vulnerable to high wind events, such as hurricanes. The strong winds induced by hurricanes could cause collapses of transmission towers and break conductors [5]. Hurricane Harvey in 2017 led to over 850 transmission structures downed or damaged and caused damages to over 1200 km of transmission and distribution conductors [6]. Hurricane Sandy in 2012 caused over 200 transmission line failures [7].

To address the challenge, recent research has focused on the performance and resilience of power transmission networks under hurricanes. At the component level (transmission towers and conductors), research has been conducted to study the behavior of structural members in power networks. Some researchers focused on the development of fragility curves for transmission towers, and most of the studies show that the behavior of transmission towers not only depends on the wind intensities, but also is heavily affected by the wind directions [8]. To assess the structural performance of a transmission tower probabilistically, some researchers studied the uncertainties in the wind turbulence using dynamic simulations [9], while some others focused

* Corresponding author.
E-mail addresses: lim215@lehigh.edu (L. Ma), vasileios@fcm.com (V. Christou), paolo.bocchini@lehigh.edu (P. Bocchini).

https://doi.org/10.1016/j.ress.2021.108072
Received 25 November 2020; Received in revised form 14 September 2021; Accepted 15 September 2021
Available online 22 September 2021

on the uncertainties from structural capacities [10]. Fu and Li concluded that it is important to model the uncertainty in the structural capacity in order to accurately evaluate the tower behavior under wind loads [11]. Similarly, the conductor performance is affected by the wind direction and uncertainties from both wind turbulence and cable capacity. Zhang et al. proposed fragility models of conductors [5] based on a regression [12] derived from historical data. The conductor failure rate is described as a function of span length and wind intensities, while the impact from wind directions is not included. Ma et al. developed a physics-based conductor fragility model under hurricanes, in which the failure probability of conductors is computed based on span lengths, wind intensities and wind directions [13].

To map the hurricane impacts to the structures in the power transmission network, it is critical to have wind field data consisting of both wind intensities and directions over the time span of the hurricane event. As the hurricane moves across the region of study, the wind speed and direction change continuously at the site of an individual tower or conductor segment due to the time-varying distance from the hurricane center and the decaying of hurricane intensity. This time-varying effects may substantially impact the probability of failure of the structures because of two reasons. First, the structure may fail at any moment during the hurricane, and only considering its failure at a particular time instant, such as the time when the structure experiences the largest wind intensity, may not reflect the performance of the structure in reality. Second, the structural failure depends on the combined effect of wind intensity and direction. The structure may be more vulnerable under smaller wind intensity with unfavorable wind direction compared to larger wind intensity but in a more favorable direction that results in small wind load on the structure. Therefore, time-varying effects, which take the combined information of wind intensities and wind directions into consideration during the entire time span of the hurricane event, should be considered for the failure probability assessment. However, some popular hurricane databases, such as the one associated with Hazus [14], only provide the maximum wind intensities during the hurricane for a relatively low resolution in space, while the corresponding wind directions and time-varying features are not included. Therefore, more comprehensive hurricane data are needed to conduct realistic simulations for structural performance assessment in power transmission networks. It is note that, this research focuses exclusively on structural failures and disregard the electrical faults that can happen in a hurricane event due to lightnings. Unlike the power distribution network which is prone to failures due to falling trees and flying debris, these events are rare for power transmission network [15,16]. Therefore, those failure modes are not considered in this research.

At the system level, some comprehensive frameworks are developed to rank the critical components and assess the system performance of the power network. However, limited research considered the structural behavior of the components, and even fewer studies addressed the combined effects of the wind speed and direction on the structures, let alone the time-varying effects. Zio and Golea analyzed the power transmission system based on topological and electrical analysis [17]. Ouyang and Duenas-Osorio developed a hurricane resilience assessment framework for electric power systems in which the component failure is computed based on the empirical fragility model with maximum wind speed as the only demand parameter [16]. In more recent studies, the structural component failure in the power network was studied considering the wind direction and time-varying effects [5,18]. However, these studies simplified the computation of the structures failure probabilities by ignoring the uncertainties in the structural capacities. This may be partially due to the fact that the fragility models developed with uncertainties on the structural capacity are incompatible with the time-varying analysis, since the capacity of an individual structure is constant during the hurricane. In addition, another simplification was made in these studies by assuming that all structures have independent probability of failure, and thus the correlations among structures was ignored. For the electrical analysis, which is used to measure the system performance by computing the unmet demand in the network considering cascading failure, researchers proposed various methodologies that are based on different assumptions [16,19–21]. A variety of these methods are reviewed by Vaiman et al. [22]. In this research, the alternate current based method proposed by Li et al. [23] is adopted.

Table 1
Definitions of some nomenclatures.

Nomenclature	Definition
Structural members	The element forming each structure, such as legs in a tower or wires in a cable
Structures	Transmission towers, conductor cables, distribution poles, etc.
Transmission line	The set of conductor cables and transmission towers connecting two transmission sites
Power network	The entirety of the transmission sites and transmission lines

The majority of the studies on power network performance are based on projecting a simplified synthetic power network, such as the IEEE bus systems whose real geographical location are undefined, to the study region [5,17]. Some researchers utilized synthetic power transmission networks developed specifically for the study region [15,16,24], however, these networks are often developed by local utility companies with focus on the electrical properties of critical nodes in the power network, such as the power plants and substations. The detailed information for the structures, such as the latitude and longitude of the towers and the length of the conductor segments are not included, and have to be assumed by the researchers. As a result, the accuracy of the component analyses and the system analyses may be undermined.

To address the challenges mentioned above, this paper proposes a novel power transmission network performance simulation framework, and its flowchart is described in Fig. 1. In this paper, the methodology is demonstrated for a study region in the Lehigh Valley, Pennsylvania, using a component-centric model of the power transmission network (Section 2). A hurricane simulator developed by the research group [25] is utilized to simulate a specific hurricane scenario affecting the study region (Section 3). For any given simulated scenario, the hurricane wind fields consisting of wind intensities and directions are assessed directly at the exact positions of the structures at different time instances during the hurricane. The geographical data are obtained for all structures and transmission line paths in the network based on a year-long data collection and image processing campaign to reflect the realistic properties of the network. A method based on a pool of component fragilities computed with different capacities is proposed to make the time-varying analysis compatible with the uncertainty model of structural capacities (Section 4). Moreover, a random field based technique is utilized to efficiently model the correlation among structural damage states (Section 5). From the damage of individual structures, it is possible to determine the functionality of an entire transmission line, and the way in which it evolves during the hurricane event (Section 6). The electrical power flow analysis is carried out in this research by means of an alternate current optimal power flow model, and the power network performance is assessed using Monte Carlo simulation (Section 7). Finally, Section 8 summarizes the main contributions and findings of the paper. Table 1 shows the definitions of some terms used throughout the paper.

This proposed scenario-based framework can be considered as part of the procedure to compute the long-term risk of a power network under hurricane events. The complete procedure to estimate long-term hurricane risk is described in Fig. 2. The proposed framework should be used in the second step for loss estimation based on the selected hurricane scenarios. The proposed framework can also be used to evaluate and visualize the system and component performance under benchmark scenarios, and help decision makers develop long-term strategies to increase the system resilience.

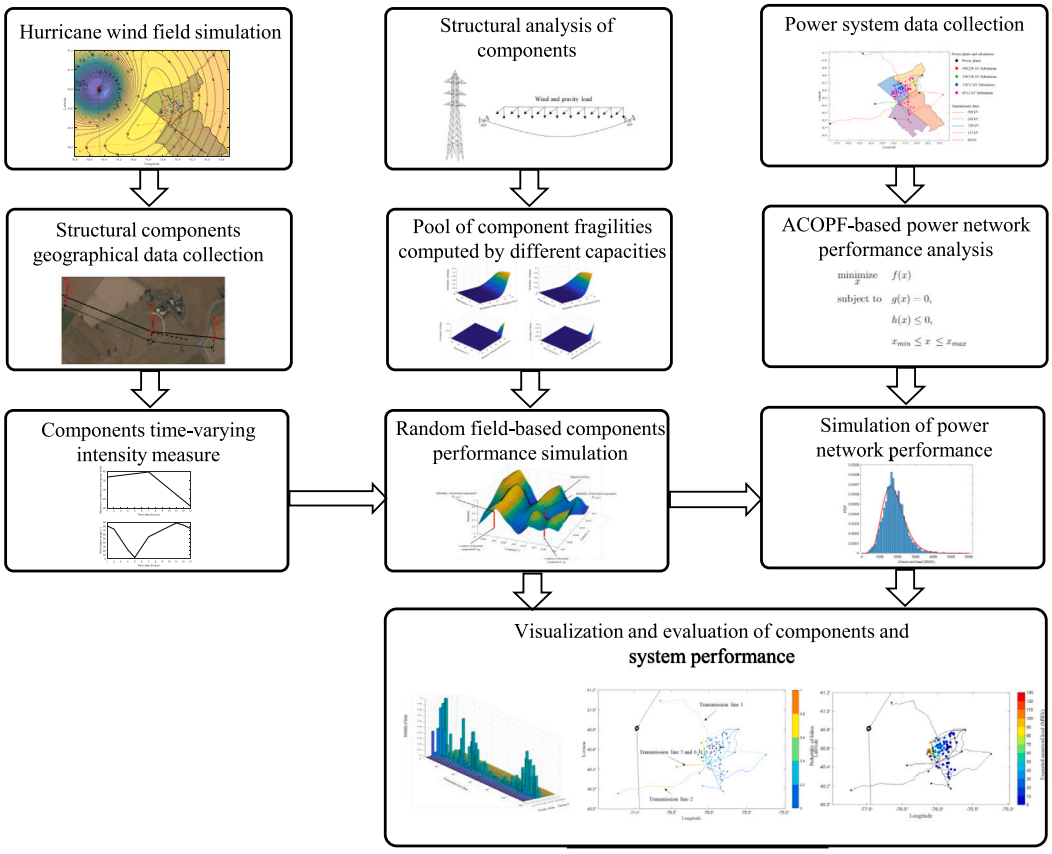

Fig. 1. Flowchart of the power transmission network performance simulation framework.

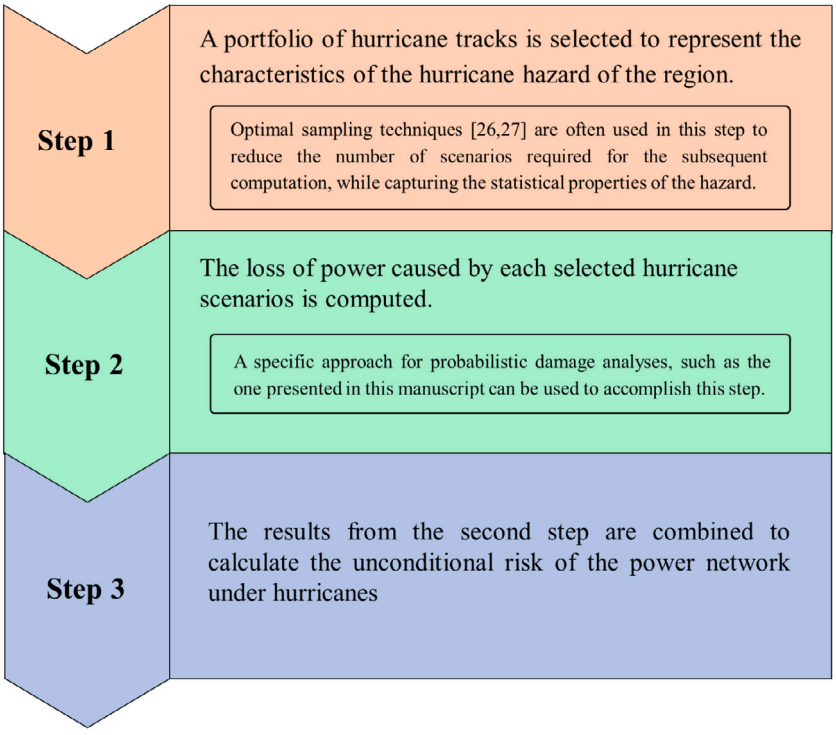

Fig. 2. Steps to estimate the long-term regional hurricane risk of power transmission network.

Table 2
Area and housing units for the counties within the study area.

County	Housing units density (per square miles)	Area of the study region (square miles)	Customers within the study area
Lehigh	413.2	277.84	114,803
Bucks	407.0	192.02	78,152
Northampton	325.6	322.76	105,090
Montgomery	674.3	23.37	15,758
Total	1834.7	816.00	313,803

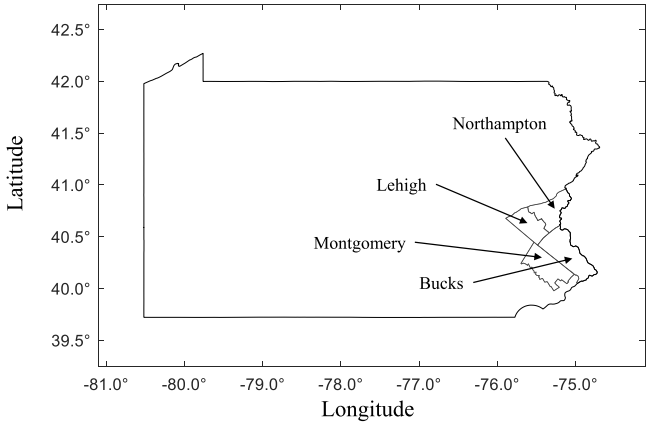

Fig. 3. The study region inside the state of Pennsylvanian.

Thanks to the recent technology development, the trajectory of the approaching hurricane track can be predicted by the National Hurricane Center several days ahead of landfall. Therefore, the results of the simulation can help decision makers optimize the short-term resource allocation strategy to effectively reduce the impact of an approaching hurricane.

2. Component-centric synthetic power network model

While the proposed approach is general, it is demonstrated in this paper on a specific study region, with clear administrative boundaries. The study area for this research is the Lehigh Valley region in eastern Pennsylvanian, including Lehigh County, Bucks County, Northampton County and Montgomery County. The location of the study region with respect to the state is showed in Fig. 3. One of the goals of this study was to develop a synthetic power network model that could match the size and characteristics of the actual power grid in the region. The electricity demand within the study area is computed based on the corresponding population of each postal code. The area and housing unit data obtained from US Census Bureau [26] within the study area are listed in Table 2. As shown in the table, the total number of households in the study area is calculated using the area and housing density of the each county. Based on our conversations with the local utility company, the peak demand of a household in the service area is about 4 kW. Following common practice, the total demand of the study region is estimated by computing the peak demand for all households and increasing it by 10%, which leads to 1255 MW. In reality, not all households will draw peak power simultaneously, but this overestimation of the residential power demand and the additional 10% are meant to account also for the extra power demand from non-residential units.

Table 4
Characteristics of substations within the study area.

Voltage (kV)	Number of substations	Type of substations
500	10	Transmission
230	5	Transmission
138	15	Distribution
69	52	Distribution

The power generation data is collected based on the power plants supplying electricity to the area. Table 3 shows the properties of 8 power plants within the study area. The name plate capacities of the power plants are retrieved from online sources [27–33]. The real power (P_g) and reactive power (Q_g) generated by the power plants are computed based on the name plate capacity and types of fuels used by the power plants [34,35].

The data on the substations in the region are summarized in Table 4. There are 15 transmission substations and 67 distribution substations in the study area. The total demand of the network is assumed to be divided equally among the distribution substations.

A campaign of data collection and image processing was carried out to obtain all the geographical information for the power transmission network. The latitude and longitude of all transmission towers are deduced from analysis of satellite images. Then, all the transmission towers were pin-pointed on the image, and the paths of the transmission lines could be determined by connecting those points. Fig. 4 shows the image of a part of a transmission line with the transmission towers pin-pointed. The coordinates of the transmission towers can be deduced from the image. The span length for each conductor segment is computed based on the Haversine formula and the coordinates of the transmission towers as:

$$\Delta_{lat} = Tla_i - Tla_{i-1} \tag{1}$$

$$\Delta_{lon} = Tlo_i - Tlo_{i-1} \tag{2}$$

$$dR = 2\arcsin\left(\sqrt{\sin^2(\Delta_{lat}/2) + \cos(Tla_{i-1})\cos(Tla_i)\sin^2(\Delta_{lon}/2)}\right) \tag{3}$$

$$L_{i-1} = dR \times R \tag{4}$$

where Tla_i and Tlo_i are the latitude and longitude in radians of the ith tower, respectively; L_{i-1} is the span length of the $(i-1)$th segment of the transmission line; R is the earth radius; dR is the central angle between ith tower and $(i-1)$th tower. The span length of the conductor segments vary depending on the terrain features and voltage levels. The direction of the conductor is defined as the clockwise angle between the North and the conductor segment, as described in Fig. 4. The direction of the transmission tower is estimated as the average of the directions of the two adjacent conductor segments supported by the tower. The

Table 3
Characteristics of power plants within the study area.

Power plant	Name plate capacity (MW)	Type of fuel	Capacity factor	Real power generated (MW)	Reactive power generated (MVAR)
Limerick generating station	2317			2085.3	1564.0
Susquehanna stream electric station	2600	Nuclear	90.0%	2340.0	1755.0
Three mile island nuclear generating station	837			753.3	565.0
Calpine Bethlehem energy center	1162	Combined		650.7	488.0
Gilbert generating station	438	cycle	56.0%	245.3	184.0
Martins Creek power plant	1700	natural		952.0	714.0
Ontelaunee energy facility	600	gas		336.0	252.0
Northampton coal	134	Coal	52.7%	70.6	53.0

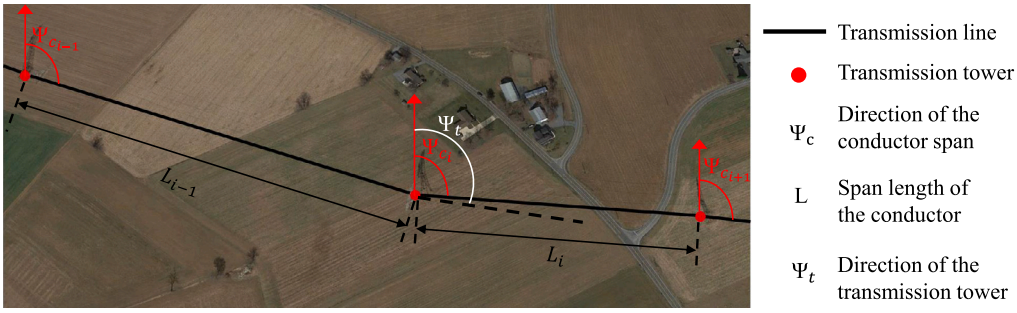

Fig. 4. Real transmission towers and conductor segments of the network.

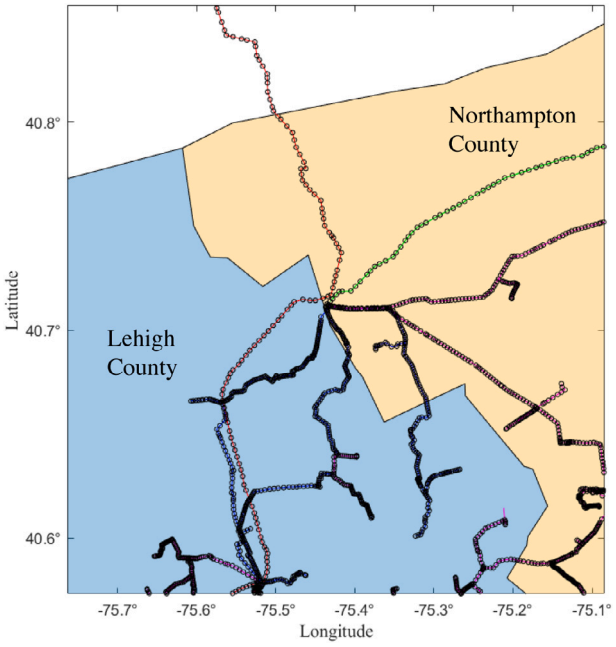

Fig. 5. Part of the power transmission network showing the towers pin-pointed along the paths of the transmission lines.

directions of the conductors and transmission towers are calculated as follows:

$$\Psi_{c_{i-1}} = \text{atan2}[\sin(\Delta_{lon})\cos(Tla_i), \cos(Tla_{i-1}) * sin(Tla_i) - sin(Tla_{i-1}) * cos(Tla_i) * cos(\Delta_{lon})]$$
$$\Psi_{t_{i-1}} = \frac{\Psi_{c_{i-1}} + \Psi_{c_i}}{2} \quad (5)$$

where $\Psi_{c_{i-1}}$ and Ψ_{c_i} are the directions of ith conductor segment and $(i-1)$th conductor segment, respectively; $\Psi_{t_{i-1}}$ is the direction of $(i-1)$th tower. Since the tower is normally designed such that the load from the two transmission lines balance and cancel out each other in the longitudinal direction, $\Psi_{t_{i-1}}$ is calculated as the average of the directions of the transmission lines connected to the tower. It is possible that minor deviations from the ideal condition occur in practice, but they are negligible, and their detection would require very high-resolution satellite images, which are not publicly available. The lengths of the transmission lines in the region are computed as the summation of the span length of the pertinent conductor segments. Fig. 5 shows part of the power transmission network with towers pin-pointed along the paths of the transmission lines. The developed Lehigh Valley power transmission network with different voltage levels of substations and transmission lines is presented in Fig. 6. In the Lehigh Valley region, there are 115 transmission lines and 5999 transmission towers. Fig. 7(a) and (b) show the distribution of the transmission lines lengths and voltage levels, respectively. The majority of the transmission lines in the region are less than 20 km, and are of voltage levels lower than 138 kV. There are two transmission lines that are longer than 100 km, and both operate at 500 kV. For each transmission line, data associated with all transmission towers and conductor segments need to be carefully collected for the subsequent assessment of the probability of failure. Special attention should be paid to some transmission towers that carry two transmission lines. These towers are critical because failure of these towers will result in failure of two transmission lines simultaneously. For example, a schematic of three transmission lines (A–B, A–C and B–C) is presented in Fig. 8. Both transmission line A–B and transmission line A–C have part of their line supported by transmission towers in Group 1. Therefore, the failure of the towers in Group 1 will result in the disconnection of transmission lines A–B and A–C. Similarly, towers in Group 3 belong to transmission lines A–B and B–C, and towers in Group 2 belong to transmission lines B–C and A–C.

To capture the effects of damage to the external transmission lines supplying power to the Lehigh Valley region, the power transmission network outside of the area of interest needs to be modeled. In this study, a hybrid model is adopted [3]. Compared to the high-resolution power network model established in the Lehigh Valley, for the area outside of the Lehigh Valley (i.e., rest of Pennsylvania and New Jersey), a lower resolution power network model, which is sufficient to capture the effects of damage to the external transmission lines supplying power to the Lehigh Valley, is established, as displayed in Fig. 9.

The number of transmission towers along a line in the low-resolution model is computed as the length of the transmission line divided by the average span length, which is set as 0.33 km, based on the data collected for the Lehigh Valley region.

3. Hurricane simulation

A hurricane simulator developed by the research group [25] is utilized to simulate a specific hurricane scenario that has significant impact on the study region. The characteristics of the simulated hurricane track are determined by physical, data-driven, and stochastic models. After origination in the Atlantic ocean, as shown in Fig. 10, the hurricane eye moves along the east coast into the Chesapeake Bay. The hurricane makes landfall in northern Maryland and continues to move North heading to the study region in Pennsylvania. The hurricane track is shown in Fig. 10 with 6-hour increments, which is the most common resolution for hurricane simulation models. It is noted that the hurricane track can be interpolated linearly or using a spline-based method. In this research, the linear interpolation is used, following the most common trends in regional loss analysis.

The locations of the hurricane center during the time span in which the study area is affected are shown in Fig. 11. The simulated hurricane track starts to threaten the power network at 12:00 September 1st (t_1). Six hours later, at 18:00 September 1st (t_7), the distance between the hurricane center and the majority of the considered power network is the smallest, and therefore the most severe hurricane impact on the

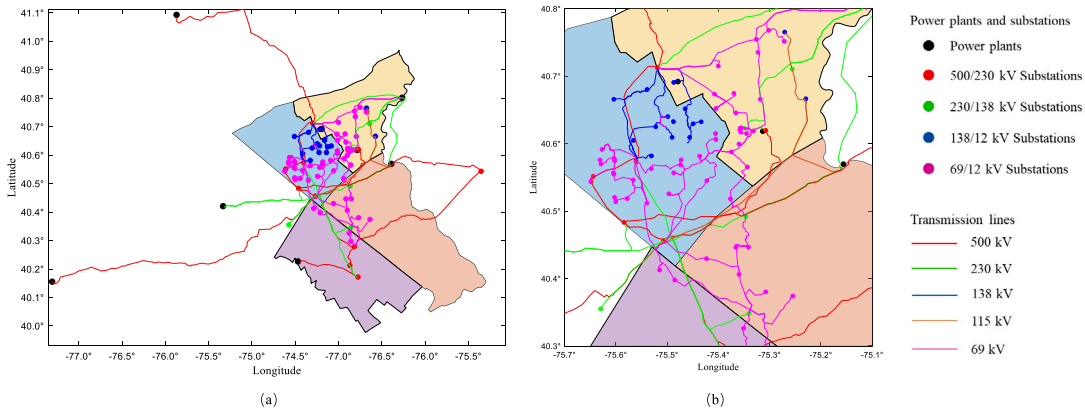

Fig. 6. (a) Lehigh Valley power transmission network (b) Lehigh Valley power transmission network (zoom in).

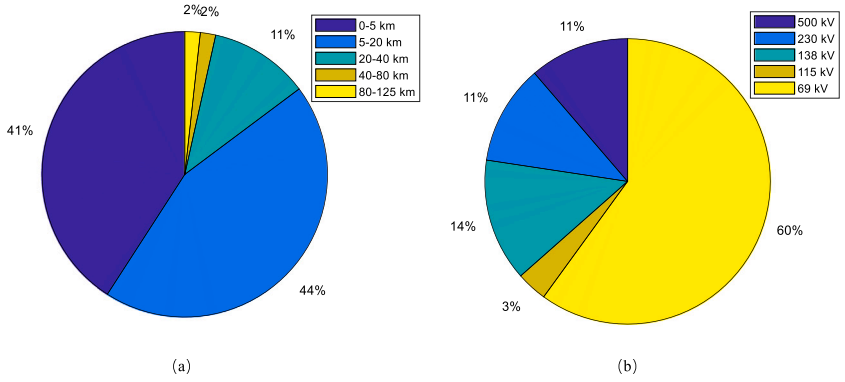

Fig. 7. Distribution of transmission lines (a) lengths and (b) voltage levels.

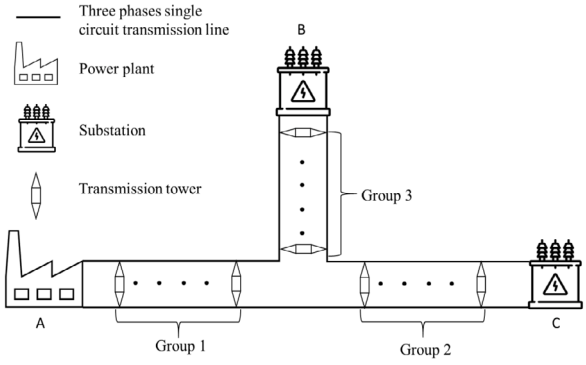

Fig. 8. Schematic of three transmission lines with shared towers.

power network is expected at this time. The hurricane is considered to be out of the study region after 0:00 on September 2nd (t_{13}).

The simulated hurricane data are summarized in Table 5. After landfall, the hurricane intensity decays over time while the central pressure increases. In this study, since the structural performance is evaluated with resolution of 1 h, the hurricane data are interpolated linearly from t_1 to t_7 and from t_7 to t_{13}.

To determine the wind speed at the locations of interest, the gradient wind speed $V_G(r,t)$ needs to be determined [25]:

$$V_G(r,t) = \frac{1}{2}(V_t \sin\alpha(t) - fr) + \left[\frac{1}{4}(V_t \sin\alpha(t) - fr)^2 + A(r,t)\right]^{\frac{1}{2}} \quad (6)$$

$$A(r,t) = B(t)\frac{\Delta p(t)}{\rho}\left(\frac{R_{wm}(t)}{r}\right)^{B(t)} \exp\left(-\left(\frac{R_{wm}(t)}{r}\right)^{B(t)}\right) \quad (7)$$

Table 5
Simulated hurricane data.

Time step	Time	Location	Maximum sustained wind (m/s)	Central pressure (mb)
t_1	12:00	39.2135°, −76.4091°	48.5901	915.2161
t_7	18:00	40.8085°, −76.4745°	40.4474	931.7094
t_{13}	00:00	42.3122°, −75.2389°	30.8246	941.4105

where V_t is the hurricane translation velocity; $\alpha(t)$ is the angle between the hurricane translation direction and the direction of the lines connecting the hurricane center to the location of interest; f is the Coriolis coefficient; r is the distance from the hurricane center to the location of interest; $R_{wm}(t)$ is the radius of maximum wind speed; $B(t)$ is the Holland B parameter [36]; ρ is the air density and $\Delta p(t)$ is the central pressure difference. The wind speed at height h above the ground can be calculated based on the hurricane boundary layer model developed by Vickery et al. [37] as:

$$U(z) = \frac{u_*}{k}\left[\ln\left(\frac{h}{z_0}\right) - a\left(\frac{h}{H^*}\right)^n\right] \quad (8)$$

where u_* is the friction velocity, k is the von Kármán coefficient, and z_0 is the surface roughness. Parameters a, n and H^* have been determined according to the methods described in the literature [37]. The wind direction at the target location defined as clockwise positive with reference to North is a function of the hurricane center to the target location and the wind inflow angle α_{SR}. The procedure to determine α_{SR} can be found in literature [38]. The wind direction at the target location α_l can be computed as:

$$\alpha_l = \alpha_t - 90 + \alpha_{SR} \quad (9)$$

where α_t is the angle between a vector pointing North and the vector with an initial point at the hurricane center and a terminal point at the

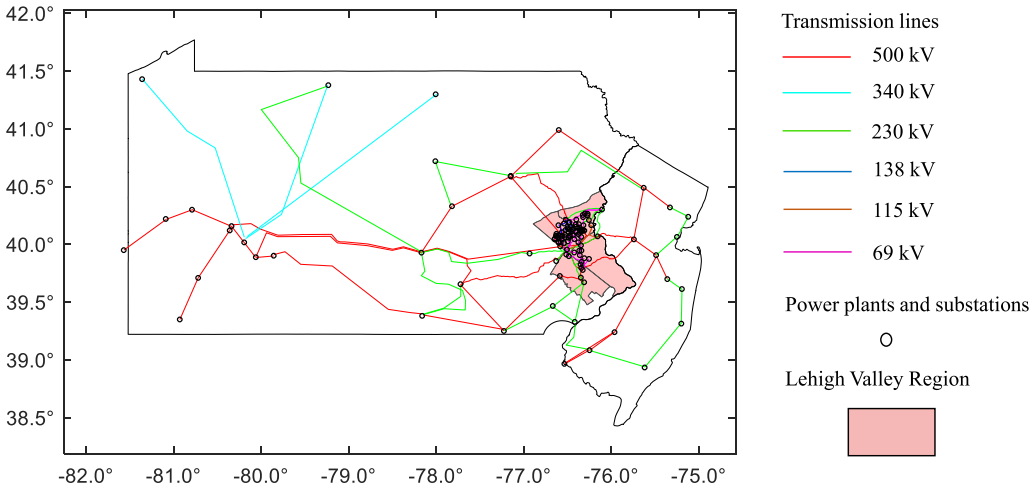

Fig. 9. Power network outside the Lehigh Valley region.

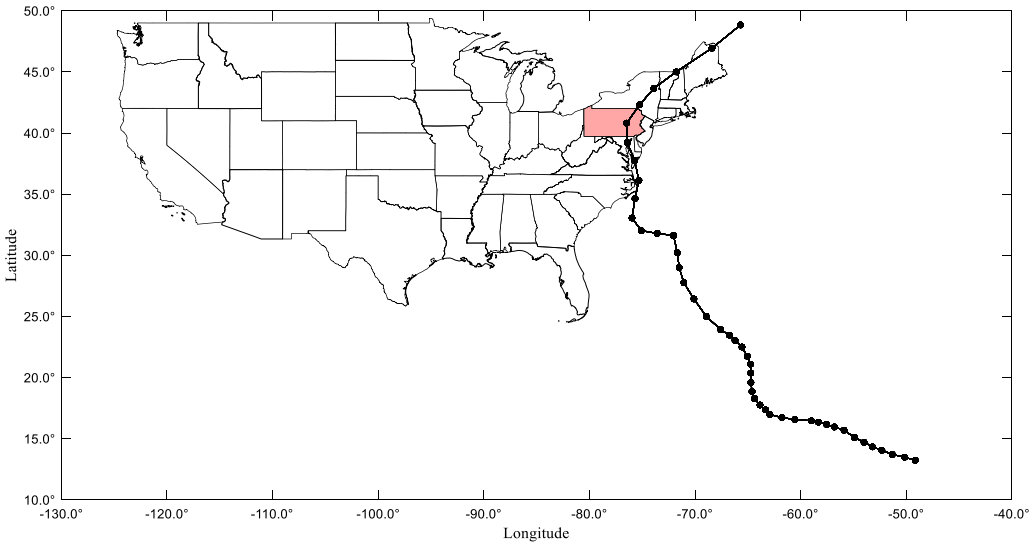

Fig. 10. Simulated hurricane track.

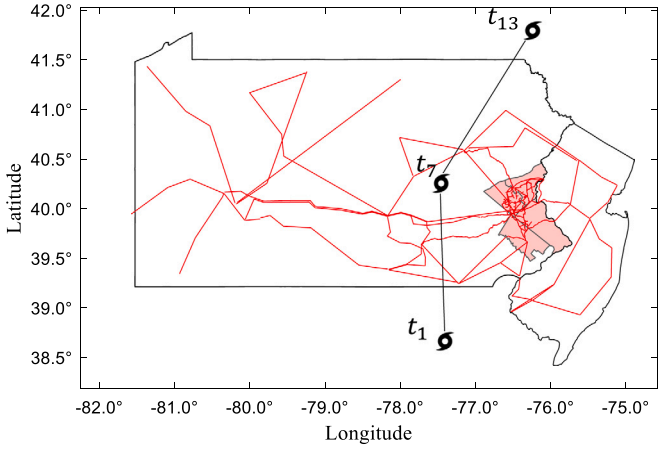

Fig. 11. Part of the hurricane track affecting the study region.

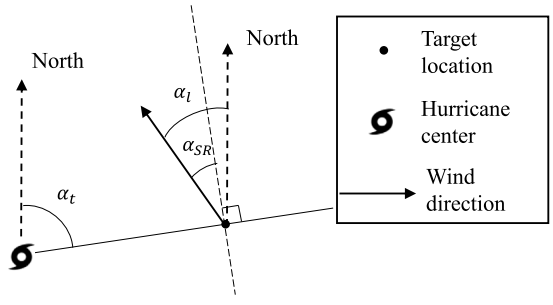

Fig. 12. Inflow angle and wind direction at a target location.

target location. Fig. 12 shows the wind direction and inflow direction for a target location.

Fig. 13(a) shows the wind field at t_1, which is the time when the hurricane makes landfall south of the study region. Fig. 13(b) highlights the spatial wind field distribution around the hurricane center. Fig. 13(c) focuses on the wind field distribution over the study region. The wind intensities are relatively low at this time step, because of the far distance between the hurricane center and the power network. Fig. 13(d) shows the field of wind direction at the study region, the majority of the power network is subjected to a wind going from

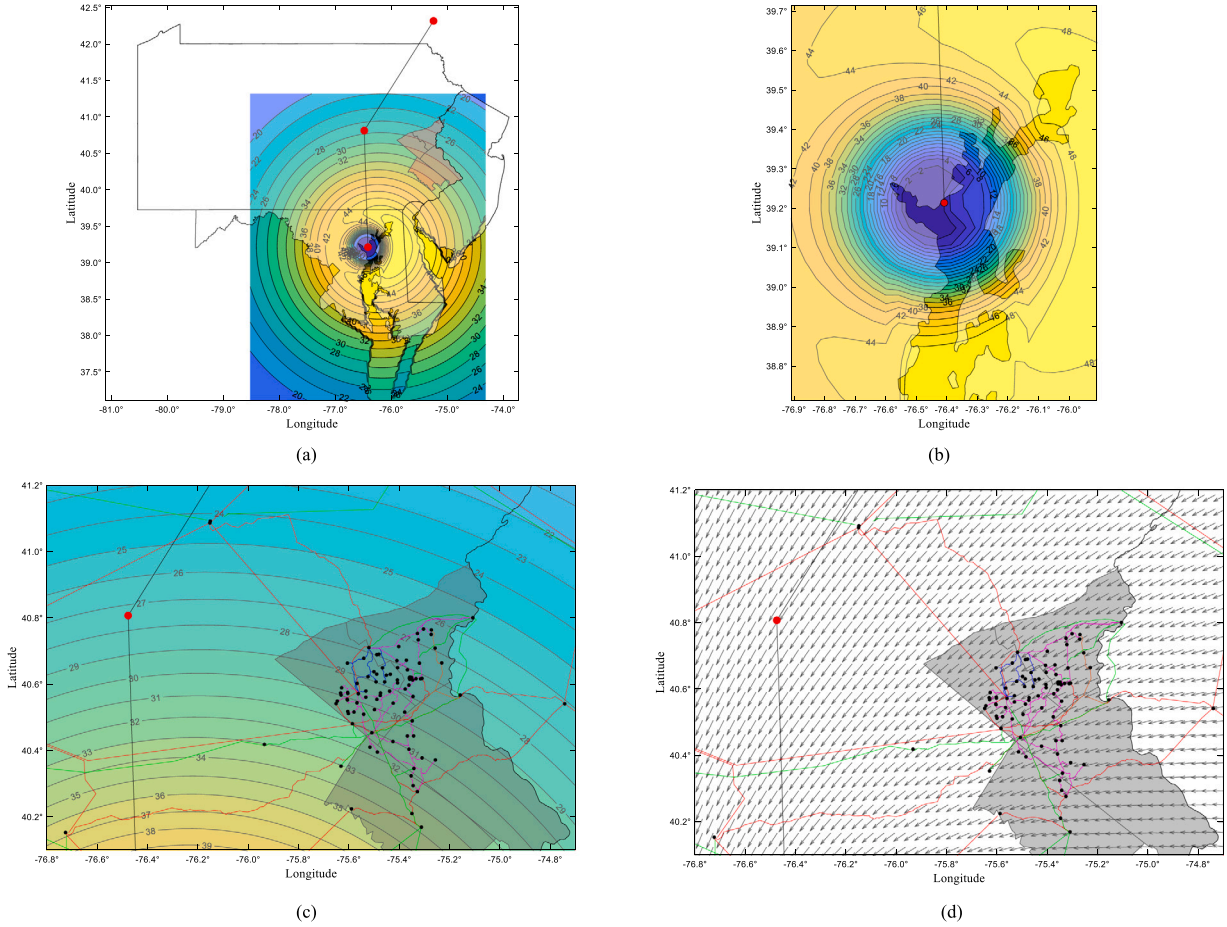

Fig. 13. (a) Hurricane wind field at time step t_1 (b) Hurricane wind field at time step t_1 zoom in at the hurricane center (c) Hurricane wind field at time step t_1 zoom in at the study region (d) Hurricane wind direction at time step t_1 zoom in at the study region.

northeast to southwest. Fig. 14 shows the wind field at t_7 when the hurricane moves further inland, and its center is positioned closer to the power network. It can be seen that the intensity of the wind field around the hurricane center has decayed compared to the wind field at t_1. However, the power network experiences larger intensities because of the smaller distance between the hurricane center to the power network. The wind direction at the study region has changed dramatically compared to t_1 and is mainly from South to Northeast at t_7. Figs. 13 and 14 show that the hurricane simulator yields asymmetric wind fields which account for the water-to-land transition and the hurricane's forward speed.

The wind attack angle is defined as the relative direction between the structures and the wind direction. Fig. 15 shows the wind attack angle computed for a transmission tower. The wind attack angle (α_k) for a structural component is computed as a function of the wind direction (α_l) and the direction of the component (α_d) as:

$$\alpha_k = 90 - (\alpha_d - \alpha_l) \tag{10}$$

where α_l is defined previously and α_d is the angle measured clockwise starting from North. For conductors, the most unfavorable wind attack angle is 0° and ±180°. For transmission towers, the most unfavorable wind attack angle varies depending on the tower design.

4. Component fragility model

Two types of structures are studied in the power network: transmission towers and conductors. The probability of failure for these structures can be evaluated and used to build fragility curves. For all transmission towers and conductors, the time-varying wind intensities and directions are obtained using the simulator described in Section 3.

4.1. Fragility of transmission towers

In the study region, different types of lattice transmission towers, H-frames and monopoles are used to support the transmission lines. In general, specific fragility models should be applied to each one of these structures, if available. For this specific study region, it was noticed that one class of structures, the lattice transmission towers, is by far the most common. A fragility model had already been developed by the authors for this class of lattice transmission towers, so for this illustrative application this fragility model is applied also to the other support structures in the region. 3D finite element models of these towers were developed and large scale dynamic simulations were conducted for the fragility curves assessment. The failure of the tower was determined through the failure of its structural members and resulting progressive collapse. The fluctuations of the wind load directly applied to the tower and transferred from the conductors were simulated by spectral representation method. The wind fluctuation samples were simulated first based on their hourly mean wind speed, and then a moving window was used to extract the maximum one minute sustained wind speed from the wind fluctuation samples. The demand distributions of the structural members were computed based on the samples generated from dynamic analyses. The capacity of the structural members were determined by the ASCE standard [39], which covers various types of members, such as legs, bracings and redundants with different types of bolted connections and eccentricities considered. The uncertainties on the member strength were modeled using empirical distributions derived from experimental campaigns [40]. Fig. 16(a) shows the geometry of the tower, and Fig. 16(b) shows the demand and capacity distributions for one main member of the tower. The failure probability

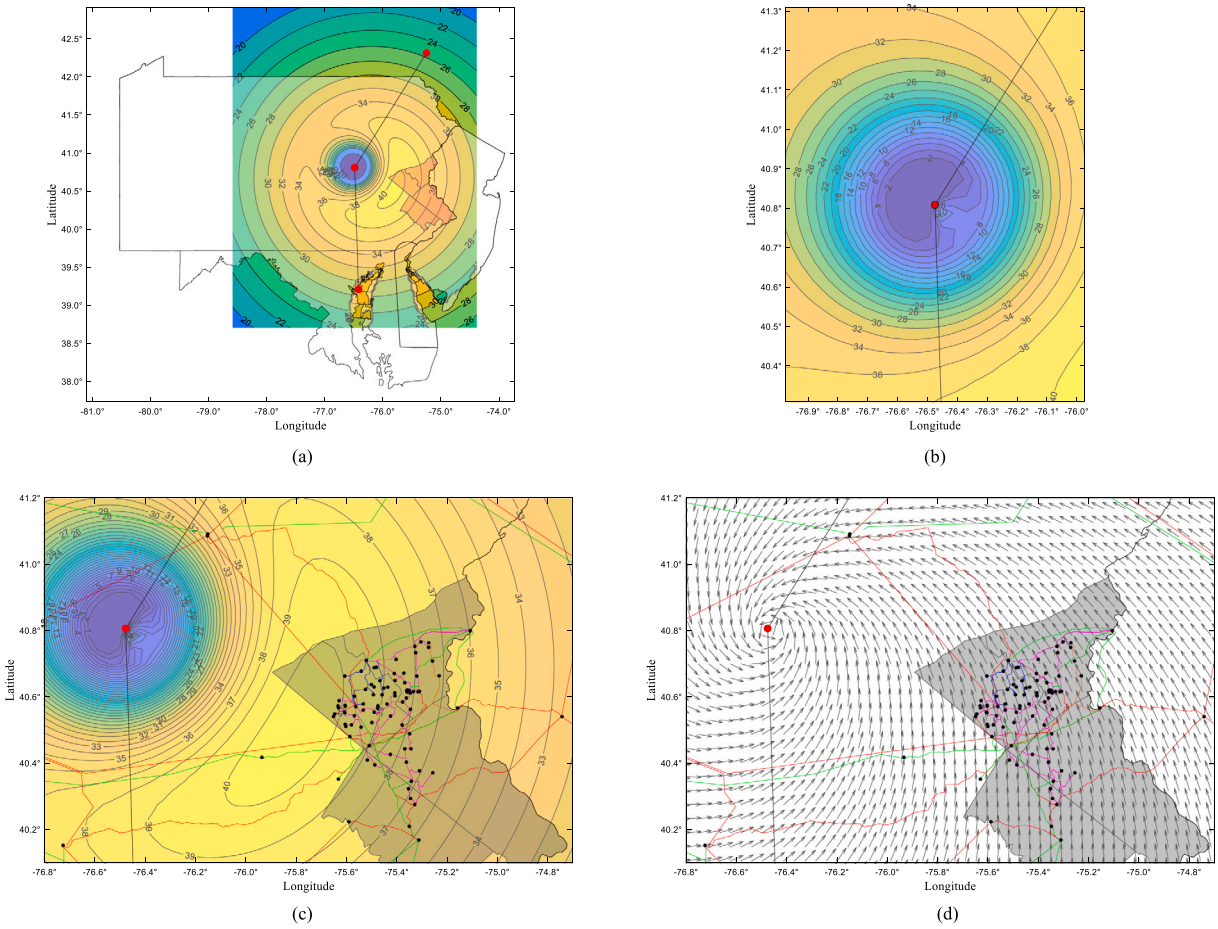

Fig. 14. (a) Hurricane wind field at time step t_7 (b) Hurricane wind field at time step t_7 zoom in at the hurricane center (c) Hurricane wind field at time step t_7 zoom in at the study region (d) Hurricane wind direction at time step t_7 zoom in at the study region.

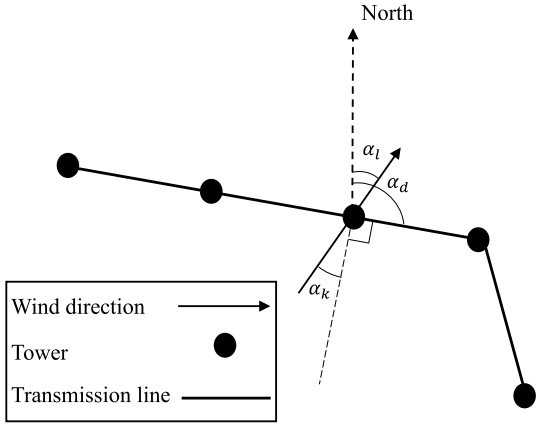

Fig. 15. Wind attack angle for a transmission tower.

of towers can be determined based on the fragility surfaces in which the combined information on the wind intensities and wind attack angles are used as demand parameters. More details of the procedure to estimate the tower fragility can be found in the literature [41]. To analyze the probability of failure of the towers during the hurricane, a discrete event simulation is carried out, where the discrete events are the failure/survival of the tower during one hour. This time interval was chosen because it is the same typically used to develop fragility curves for these structures, so the fragility curves provide directly the probability of occurrence of the event. Unfortunately, most of the fragility models found in the literature cannot be used directly because they embed the uncertainties on tower member capacity [11]. If the probability of failure was used repeatedly to sample the failure/survival of a tower at each hour using the values given by these curves, it would implicitly assume that the capacity of the tower could also change at each hour, while in reality, the capacity of an individual tower remains the same during the hurricane event. Therefore, this approach had to be modified and to consider the uncertainties in capacities in the context of time-varying analysis, the capacity and wind load uncertainties have to be studied separately. First, samples of the tower capacities are generated, and then each capacity sample is kept constant and used to generate specific fragility surfaces considering only the uncertainties in the wind loads. In this way, each fragility surface reflects the probability of failure for a certain tower capacity. A pool of 200 fragility surfaces defined as the whole sample space was generated using the procedure described in the literature [41], and for each of the transmission tower in the power network, a fragility surface was randomly sampled from the pool to represent the performance of the tower. For each tower, the goal is to have tower capacity that is consistent over time, so that each simulation represents what would happen in the reality for the power network. This is also useful for various types of analysis, such as recovery analyses. Fig. 17 shows two transmission tower fragility surfaces sampled from the pool. It is note that the fatigue failure is not considered in this study, because the fatigue damage is caused by the cumulative effect of stress fluctuations from less severe but more frequent wind events compared to hurricanes.

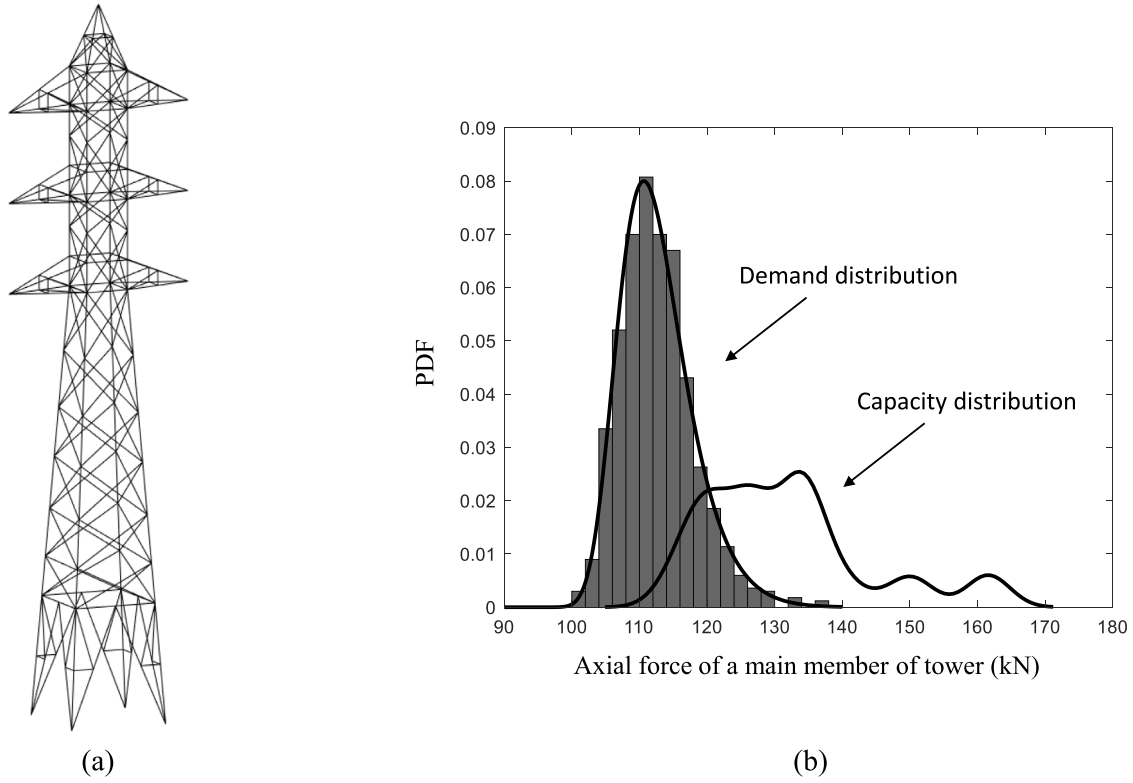

Fig. 16. (a) Geometry of the lattice transmission tower model (b) Demand and capacity distributions of the main member of the tower.

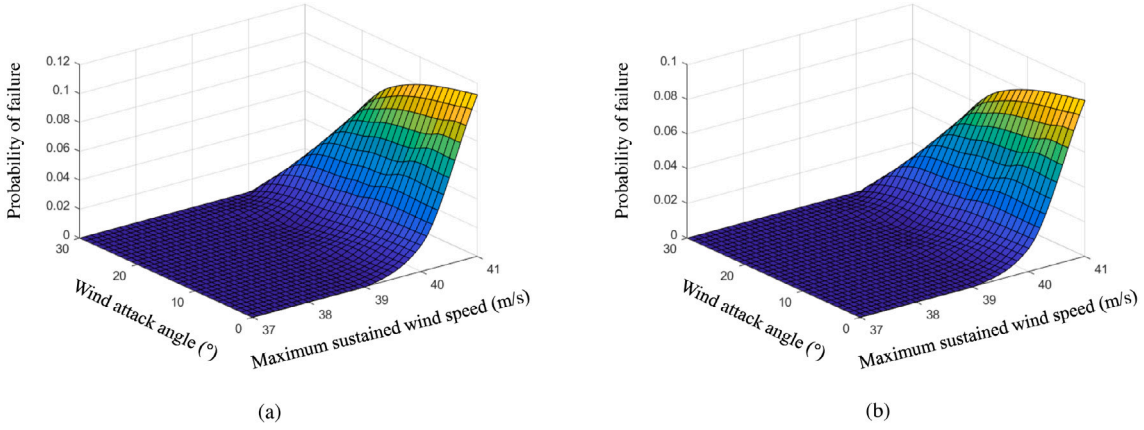

Fig. 17. (a) Transmission tower fragility surface sample N_1 (b) Transmission tower fragility surface sample N_2.

4.2. Fragility of conductors

Aluminum conductor steel-reinforced (ACSR) is widely used type of cable in power transmission network. ACSR provides higher tension, less sag and longer span lengths than all-aluminum conductors (AAC) and all-aluminum alloy conductors (AAAC). The power network consists of conductors with voltage level of 500 kV, 230 kV, 138 kV, 115 kV and 69 kV. The sizes, typical normal ratings and ampacity of ACSR to be used for specific voltage levels are demonstrated in Table 6. These information is obtained from the local utility company to reflect the real properties of conductors in the study region. The failure probability of the transmission conductors depends on the uncertainties in the wind turbulence and conductor capacities. The modal superposition method was used to model the mechanical response of the conductors efficiently, and was validated by nonlinear finite element analysis [42]. The first order reliability method was implemented to capture the low failure probability of a conductor with sufficient accuracy, as confirmed by benchmark Monte Carlo simulations [13]. Also in this case, for this specific discrete-event simulation analysis the uncertainties in the conductor capacity and demand had to be decoupled. The uncertainties

Table 6
Properties of conductors.

Voltage (kV)	Conductor size (kcmil)	Typical normal rating (MVA)	Ampacity (amps)
69	556	85	655
115	795	175	810
230	1590	650	1245
500	2156	1625	1470

of the conductor capacity was modeled by ASTM rule as:

$$CR_i = n_{aw} s_{(aw)} \frac{\pi d_{(aw)}^2}{4} + n_{sw} s_{(sw.1\%)} \frac{\pi d_{(sw)}^2}{4} \tag{11}$$

where CR_i is the ith realization of the conductor capacity; d_{aw} and d_{sw} represent the aluminum wire diameter and steel wire diameter respectively; $s_{(aw)}$ is the breaking stress of individual aluminum strands; and $s_{(sw.1\%)}$ is the stress in the steel strands at 1% extension. d_{aw}, d_{sw}, $s_{(aw)}$, $s_{(sw.1\%)}$ are all random variables with truncated normal distribution. n_{aw} and n_{sw} are the number of aluminum wires and number of steel wires, respectively. The parameters of these distributions were estimated empirically by Farzaneh and Savadjiev [43]. Similar to the transmission towers, samples of capacities were generated for each type of conductors to build the fragility pools. In reality, one conductor may extend through several segments supported by multiple suspension towers between two tension towers. Therefore, these conductor segments share the same capacity. The direction of the conductor segments are recorded as discussed in Section 2, and the tension towers are identified as the towers for which the change of directions between two adjacent conductor segments is larger than 5°. If the transmission line is single circuit with 3 conductors on one tower, for the conductor segments between two tension towers, 3 samples of fragilities are drawn from the pool. If the transmission line is double circuit with 6 conductors on one tower, for the conductor segments between two tension towers, 6 fragilities are drawn from the pool. Fragility pools of four types of conductors associated with different voltage levels are generated. Each fragility pool consists of 200 fragilities. Fig. 18 shows fragilities drawn from the pool for two types of conductor at 69 kV and 115 kV, respectively. In the developed model, the probability of failure is a function of three parameters, which are the wind speed, wind direction and span length, but for visualization purposes the fragility surfaces are showed with span length kept as constant.

It is noted that the wind time histories used for developing the fragilities are selected as the most critical period during 1-h of hurricane wind fluctuations, as customary in wind engineering [5]. This means that the resulting fragility reflects the failure probability during a particular hour of the hurricane. This probability needs to be combined with the possible failures during the rest of the hurricane event.

5. Random field based network components failure simulation

The structures need to be evaluated individually to estimate their damage states in the hurricane scenario, but the overall performance of the power network depends on a complex combination of the damage states of all its structures. Structures that are relatively close to each other in the power network are likely to share some characteristics, such as the age, construction techniques, and materials. Moreover, the wind effect is captured using only the sustained speed and direction, but towers that are close to each other will experience winds with very similar characteristics, beyond the sustained speed and direction, also due to terrain features. Hence, to accurately assess the performance of the network, this spatial correlation between the structural capacity and demand needs to be considered.

In this study, this correlation is modeled and simulated based on the random field technique proposed by Bocchini et al. [44]. The external stressors on the transmission towers and conductors are simulated as a two-dimensional non-Gaussian, homogeneous random field $d(\mathbf{x})$. The marginal distribution of $d(\mathbf{x})$ is uniform in the interval $[0, 1]$. For every time step t considered in the study, a set of samples $d_{t,i}(\mathbf{x})$ of the random field can be generated. The auto correlation function A, which is used to compute the covariance matrix needed for the generation of the random field $d_{t,i}(\mathbf{x})$ can be computed as:

$$A(\xi_x, \xi_y) = \sigma^2 \exp\left(-\frac{\xi_x^2 + \xi_y^2}{\lambda^2}\right) \tag{12}$$

where ξ_x and ξ_y are the separation distances between two locations measured along two perpendicular directions x and y, respectively; σ^2 is the variance of the marginal distribution. In this research, the external stressors on the transmission towers and conductors are represented as a two-dimensional non-Gaussian, homogeneous random field. Eq. (12) is an exponential form of autocorrelation function which was found to be appropriate for regional damage analyses of bridges under seismic events [45]. Therefore, this functional form is adopted in this study as a convenient solution to introduce in the model the desired correlation at a certain time instant. In reality, the towers and conductors connected to the same tension tower are likely to share the same structural characteristics and the same terrain and environmental features. The average distance between two tension towers in the study region is d_{ts} = 0.75 km. Therefore, towers within the distance of $2d_{ts}$ should have some degree of correlation. In this study, a value of 0.5 is assumed for the correlation coefficient of the state of structures with a distance of $2d_{ts}$. As a result, the correlation distance needs to be set to λ = 3.0 km, according to Eq. (12). A comprehensive study on the correlation distance in the context of hurricane events requires a large amount of detailed data and simulations of multiple scenarios; therefore, it is out of the scope of this research.

To generate random field samples, the entire study region is discretized with a regular grid, and the random field samples are generated using UQLab [46] given the computed covariance matrix and the marginal distribution. Then, the value of the random field at the location of a structural component can be computed by interpolation. The damage state of each structural component in the study region is given by

$$s_{c,i}(t) = \min\Big(s_{c,i}(t-1), \mathcal{H}[R_{el\,c,i}(t) - d_{t,i}(\mathbf{x}_c)]\Big) \tag{13}$$

where $s_{c,i}(t) = 0$ if structural component c of sample i is out of service at time t; $s_{c,i}(t) = 1$ if structural component c of sample i is in service at time t; $\mathbf{x}_c$ is the location of component c; $\mathcal{H}[\cdot]$ is the Heaviside unit step function, $R_{elc,i}$ is the reliability (i.e. probability of survival) of structure c of sample i at time t, and $d_{t,i}(\mathbf{x}_c)$ is the value of sample i for time t of the random field at location $\mathbf{x}_c$. Fig. 19 provides a graphical representation of Eq. (13). For each sample i and time instant t, if the reliability of structural component c is larger than the value of the random field at that location, the structural component survives (i.e., $s_{c,i}(t) = 1$), otherwise the structural component has failed (i.e. $s_{c,i}(t) = 0$). Given that the structural component is in service at the previous time step, if the structural component reliability at time t is larger than the corresponding value of random field $d_{t,i}$, the structural component survives at time t, otherwise it is failed. For instance, as shown in Fig. 19, $R_{elA,i}(t) > d_{t,i}(\mathbf{x_A})$, therefore structural component A survives at time t. In contrast, $R_{elB,i}(t) < d_{t,i}(\mathbf{x_B})$, therefore structural component B fails at time t. The value of the reliability of each structure reflects the individual failure probability due to wind intensities, wind attack angles and structural characteristics during 1 h. The random field, on the other hand, reflects the correlation among the damage states of structures in the power network.

6. Time-varying transmission line failure model

Once the simulated hurricane wind field and the structures in the power system are defined, the time-varying probability of failure for each structures in the power network can be computed. Fig. 20 shows the locations of two towers, selected among all those under investigation. Fig. 21 shows the wind intensities and wind attack angles for these two transmission towers as they evolve over time. The time-varying probability of failure of the towers is computed based on a fragility surface sampled from the fragility pool as discussed in Section 4. It should be noted that the probability of failure is associated with a discrete event for each time step, and it reflects the failure probability during that hour. The continuous line in the plot is to demonstrate the trend of the changing probability of failure. It does not indicate

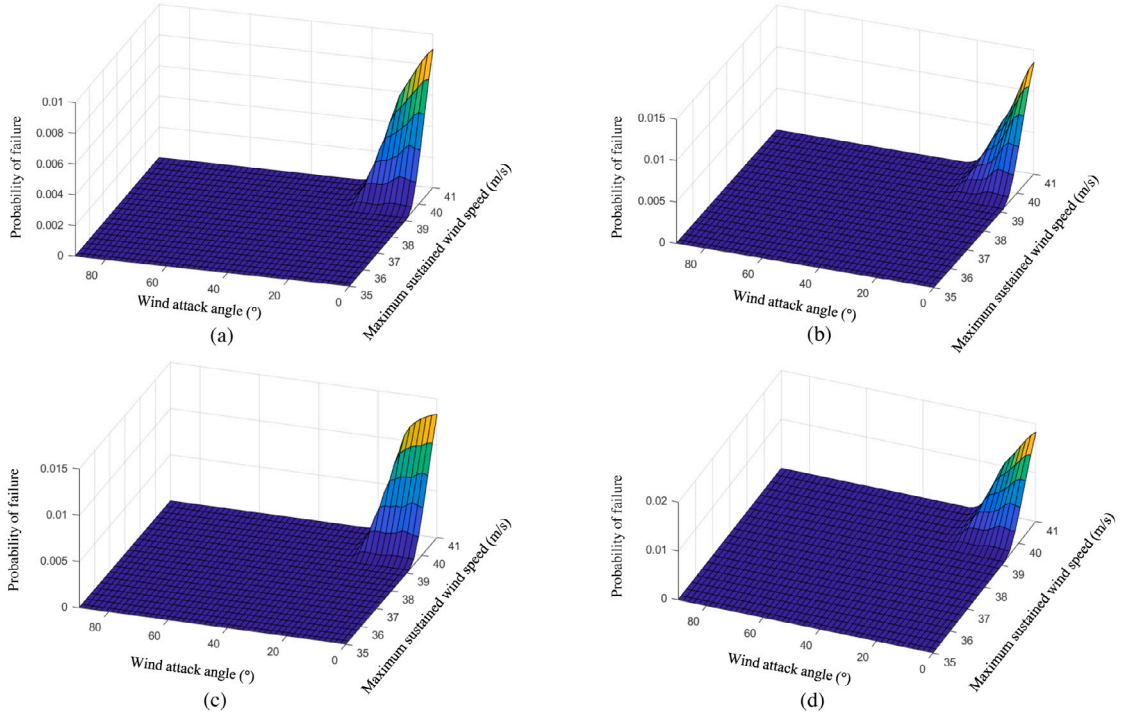

Fig. 18. (a) 69 kV conductor fragility surface sample N_1 with span length of 350 m (b) 69 kV conductor fragility surface sample N_1 with span length of 375 m (c) 115 kV conductor fragility surface sample N_1 with span length of 340 m (d) 115 kV conductor fragility surface sample N_1 with span length of 355 m.

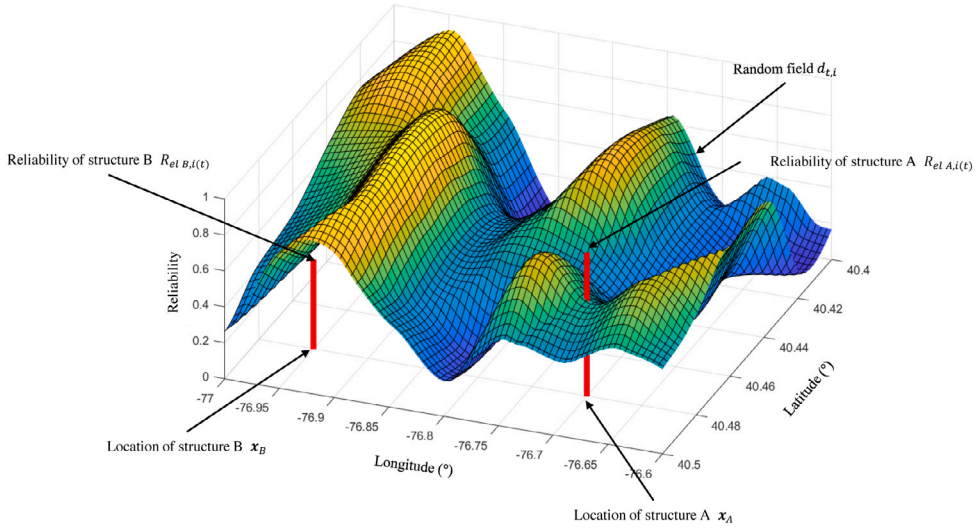

Fig. 19. Schematic graphical representation of Eq. (13) for a specific sample i (zoom in for part of the region).

that the probability of failure is continuous. As shown in Fig. 21, even though these two transmission towers belong to the same transmission line, they have different time-varying probability of failure. The largest probability of failure happens at t_5 for Tower A, while for Tower B, the largest probability of failure happens at t_7. It can be seen that the wind attack angle plays a significant role in determining the failure probability. For instance, at t_7, Tower A and Tower B are subjected to similar wind intensities, but the wind attack angle for Tower B is smaller than that of Tower A, resulting in a larger probability of failure for Tower B. More importantly, for Tower A the probability of failure at t_7, when the tower experiences the largest wind intensity, is lower than the failure probability computed at t_4, t_5, and t_6. This proves that only considering the maximum wind speed during the hurricane and its corresponding wind attack angle may lead to underestimation of the failure probability. Therefore, it is necessary to include the time-varying effects in determining component damage states. Scalar fragility curves are a function of a single parameter (the intensity measure) which should capture the least favorable loading condition over the entire event. Vector fragilities generalize this concept, trying to capture the characteristics of the event not with just one value, but more than one. In this paper, a vector fragility is considered, where the two parameters are wind direction and velocity. When a vector fragility is used, it is not obvious which combination of intensity measures will be the least favorable for a structure during an event. This last aspect leads to the necessity to repeat the fragility analysis during the multiple phases of the event, studying the various combinations of intensity measures to which the structure is exposed.

As discussed in Section 2, a transmission line, which is a serial system, may consist of hundreds of conductor segments and towers.

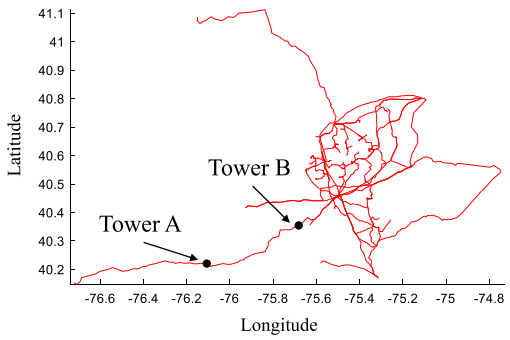

Fig. 20. Locations of Tower A and Tower B under investigation.

A transmission line survives a wind load only if all of its structures withstand the wind load; hence, the damage state of a transmission line is determined by evaluating the damage states of all its structures. Due to the various correlations introduced in the model, it is not possible to simply compute the probability of survival of the transmission line series system by multiplication, it is instead computed by Monte Carlo simulation. The simulation procedure consists of using the component fragility models and the random field technique introduced in Sections 4 and 5, respectively. The damage state for the transmission line is computed as:

$$s_{K,i}(t) = \min\left\{ s_{K,i}(t-1), \mathcal{H}\left[\sum_{j=1}^{\hat{c}} s_{c,j}(t) - \hat{c}\right]\right\} \tag{14}$$

where $s_{K,i}(t) = 0$ if transmission line K of sample i is out of service at time t; $s_{K,i}(t) = 1$ if transmission line L of sample i is in service at time t; $\hat{c}$ is the number of structures belonging to transmission line K. First, N_p samples of power network need to be generated. For each sample of the power network, fragilities for all its structures are sampled from the fragility pools. Then, for each sample of the power network, N_s simulations are conducted using the random field technique. The total number of Monte Carlo simulation conducted is $N_t = N_p N_s$. The simulation is stopped when the probability of failure for all transmission lines is stable (i.e., changes by less than 1.5%) for the last 20% samples. In this study, convergence is met when $N_t = 4000$ with $N_p = 100$ and $N_s = 40$. Fig. 22 shows the convergence of failure probability for all transmission lines in the study region.

The failure probabilities over the entire duration of the hurricane event for the various transmission lines are shown in Fig. 23. The majority of the transmission lines have probability of failure lower than 20%, while there are a few transmission lines with probability of failure larger than 60%, and there are 9 lines having probability of failure larger than 80%. As expected, the vulnerability of the transmission lines is highly dependent on their relative distance from the hurricane center. Those transmission lines that are far from the center of the hurricane are subjected to relatively smaller wind intensities, and therefore they have much smaller probabilities of failure compared to the lines that are closer to the hurricane track. The vulnerability of the

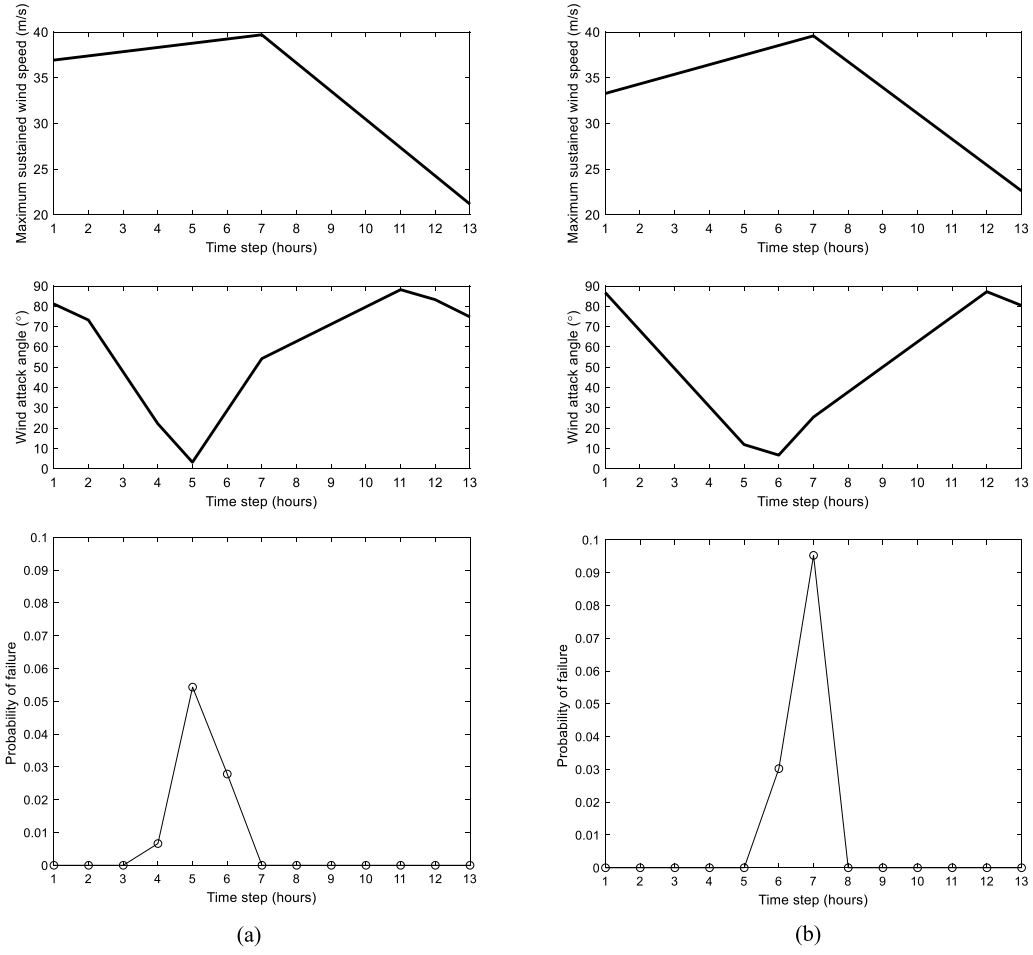

Fig. 21. (a) Time-varying wind intensities, wind attack angles and probability of failure for Tower A (b) Time-varying wind intensities, wind attack angles and probability of failure for Tower B.

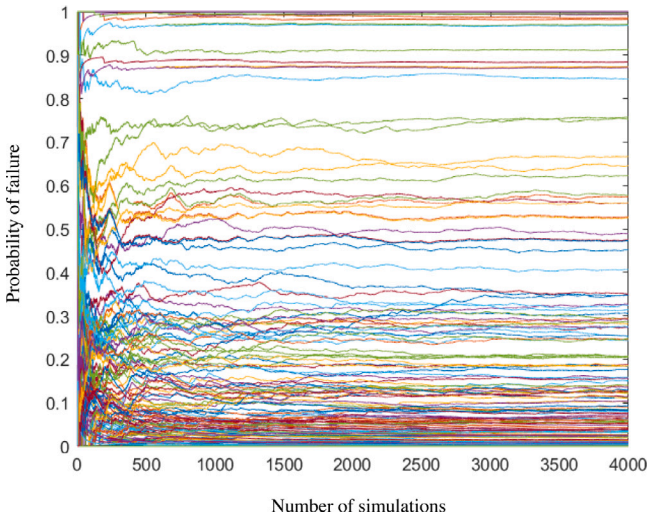

Fig. 22. Convergence of probability of failure for all transmission lines in the power transmission network.

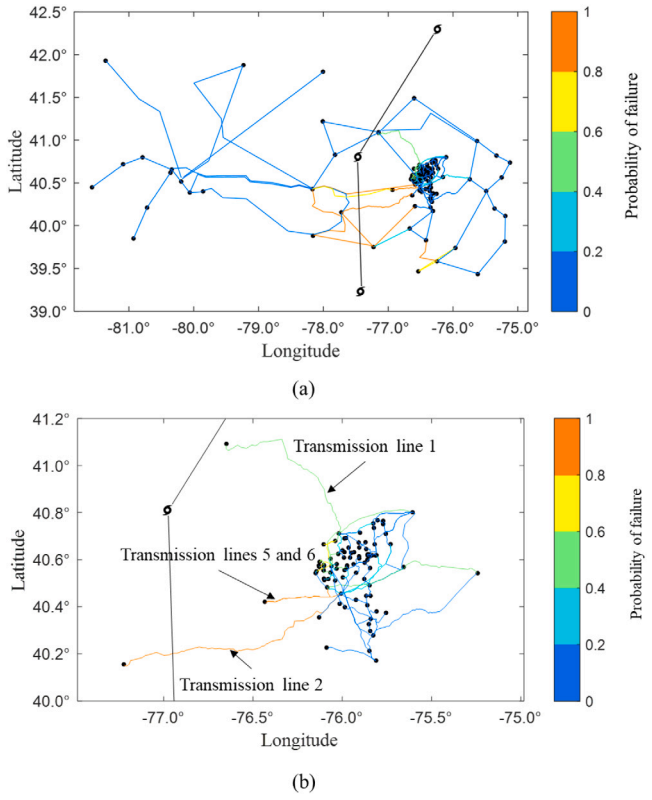

Fig. 23. Topology of the transmission lines and their corresponding probability of failure: (a) The whole network (b) Network zoom in at the Lehigh Valley region.

transmission lines is also affected by their length. However, this effect is less dominating than the wind intensities. As shown in Fig. 23(b), some short lines that are close to the hurricane center experience higher probability of failure than longer lines that are far from the hurricane eye. Transmission lines 5 and 6 are the most vulnerable lines in the network at the Lehigh Valley region, under this specific hurricane scenario. This can be partially explained by the wind field showed in Fig. 14(c) and (d). Transmission lines 5 and 6 are subjected to the highest wind intensities of the region (they cross the hurricane maximum wind radius) and almost 0° wind attack angles (worst case

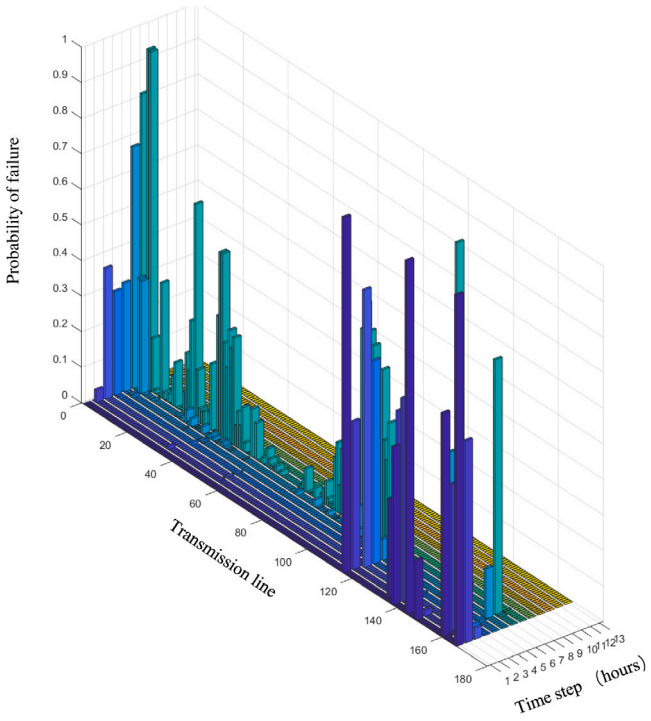

Fig. 24. Time-varying failure probability of transmission lines during the hurricane.

scenario) at the same time. Even though transmission lines 5 and 6 are not among the longest lines in the network, they are the subjected to the most unfavorable winds, which makes them the lines most likely to fail. In addition, a large part of transmission lines 5 and 6 are supported by the same group of towers, as discussed in Section 2, which could also contribute to the high probability of failure for those lines. In contrast, as shown in Fig. 14(c) and (d), when subjected to the largest wind intensity during the hurricane, transmission line 1 had a wind almost parallel to its direction (wind attack angle close to 90°), resulting in relatively low probability of failure regardless of the fact that transmission line 1 is the second longest in the network at the Lehigh Valley region.

The deaggregated and time-varying failure probability of the transmission lines during the hurricane is shown in Fig. 24. It can be seen that the hurricane starts to affect the power network at t_1, and after t_9 the hurricane has little impact on the power network. Most of the transmission lines in the Lehigh Valley region fail in a relatively narrow time period around t_7, when the wind intensities are the largest for the region. This could be explained by the relatively small area of the region and high density of the transmission lines in this region. However, there are some exceptions, such as transmission line 2, as shown in Fig. 24, which may fail over a relatively long time window starting from t_3. Transmission line 2 is the longest line in the network. As a result, different parts of this transmission line may experience the largest failure probability at different time steps. This also confirms the findings in the time-varying probability of failure for individual components, as shown in Fig. 21. Some of the transmission lines outside of the Lehigh Valley region located in Southern Pennsylvania are affected by the largest probability of failure at t_1, when these lines cross the hurricane maximum wind radius and are subjected to almost 0° wind attack angles. In addition, Fig. 24 shows that failure of transmission lines can occur at various time steps during the hurricane.

The average probability of failure for all towers in the network is 1.1087%, and the average probability of failure for all conductors is 0.0156%. As expected, transmission towers are much more vulnerable than conductors. However, the failure of the conductors may not be

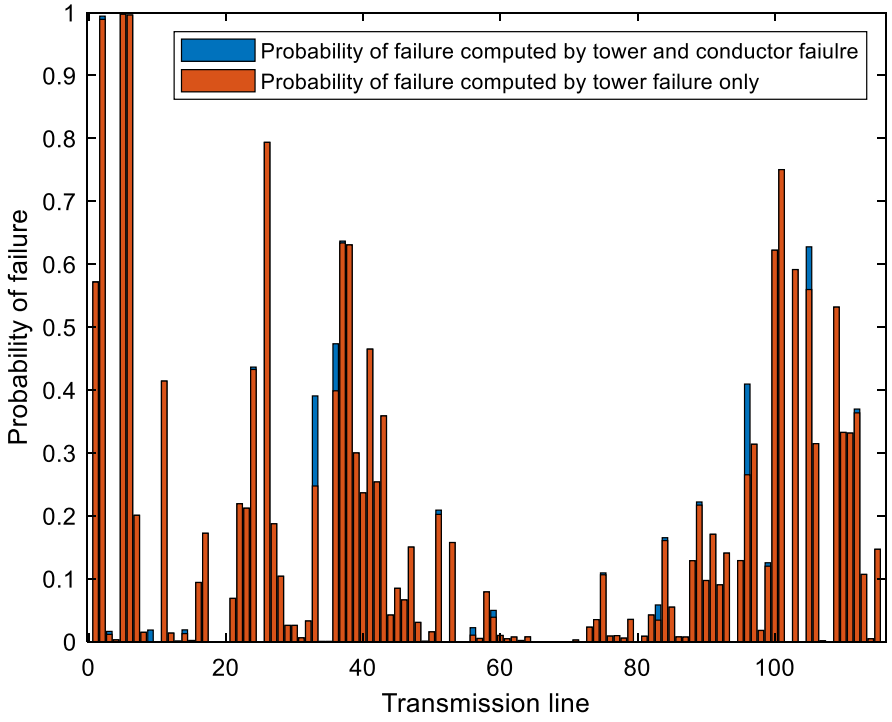

Fig. 25. Failure probability of transmission lines in the Lehigh Valley region computed by tower failure and conductor failure versus failure probability of transmission lines computed by tower failure only.

simply ignored. As shown in Fig. 25, for the majority of the transmission lines in the Lehigh Valley region, the probability of line failure computed by considering tower failures only is very close to the probability of line failure computed by considering both tower and conductor failures. For those transmission lines, the failure of the towers dominates. However, for some transmission lines the contribution of the conductor failures is not negligible. The disproportionate contribution of conductor failure to those transmission line failures can be explained by two reasons. First, the conductor fragility is "steeper" than the tower fragility, which means that the failure probability of conductors is more sensitive to the wind speed and wind attack angle, as shown in Figs. 17 and 18. So, the contribution of the conductors to the overall probability of failure is almost binary, it is either very important or almost negligible. Second, in addition to the wind intensities and wind attack angles, the failure probability of conductors is also sensitive to the span length. Therefore, in some transmission lines, the probability of failure for some particularly long conductors is comparable to the probability of failure for the towers.

7. Alternate current power network performance simulation

An alternate current optimal power flow (ACOPF) model is utilized to capture the power system response after structural failures due to hurricanes. Compared to the direct current power flow model, which is a tractable relaxation of the desirable alternate current power flow model, the alternate current power flow model is more accurate in terms of simulating the load shedding process and computing the power loss [23]. In this study, the performance of the power system is measured under the following assumptions: (a) the hurricane vulnerability of power plants and substations is negligible; (b) the damage state of the transmission line is binary: functional or failed; (c) network operators and automated switches are fast enough to interrupt power supply to certain areas to prevent further failures of the network; (d) all fast-response generating units are committed at the day of the event; (e) repair is not performed during the hurricane. In this situation, this study leverages MATPOWER [47], which is an open-source tool for electric power system simulation and optimization, to solve the ACOPF problem, carrying out an optimization aiming to maximize the total power demand satisfaction in the system. This is achieved by changing load demand at the substations and power generation at the plants, while considering all the necessary physical constraints.

The first step of the ACOPF model development on MATPOWER includes preparation of four matrices that are the bus, generator, branch and generator cost matrix. The bus matrix reflects the power demand and voltage level of the substations and the general numbering of all the power plants and substations in the network. In MATPOWER, the maximum and minimum voltage magnitude have to be predefined for each bus and these limitations are enforced during the power flow analyses. A power plant is modeled as a complex power injection at a specific bus. The maximum and minimum real and reactive power generation by each power plants are modeled in the generator matrix. All transmission lines are modeled with the branch matrix based on a standard π transmission line model with series impedance. For each transmission line, the buses it connects need to be specified in the branch matrix. The generator cost matrix consists of the cost of power production for various fuel types of the power plants. The data associated with power plants, substations and transmission lines needed for the formulation of these four matrices were obtained during the data collection campaign described in Section 2 and are summarized in Table 3, Tables 4 and 6.

The next step is to formulate the optimal power flow analysis aiming to minimize the unmet demand in the power network. The standard optimal power flow analysis takes the following form:

$$\underset{x}{\text{minimize}} \quad f(x) \tag{15a}$$

$$\text{subject to} \quad g(x) = 0, \tag{15b}$$

$$h(x) \leq 0, \tag{15c}$$

$$x_{min} \leq x \leq x_{max} \tag{15d}$$

The objective function $f(x)$ consists of the cost of generator injections; the equality constraints $g(x)$ are the power balance equations; the inequality constraints $h(x)$ are the branch flow limits, and the x_{min}

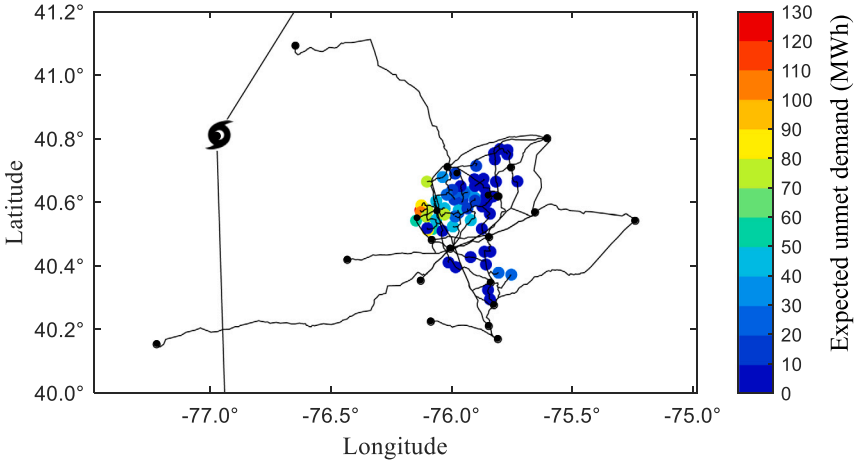

Fig. 26. Expected unmet demand for the distribution substations.

and x_{max} bounds include bus angles, voltage magnitudes and generator injections. For a standard ACOPF, the objective of the optimization problem is to minimize the power production cost. However, in this study, the power demand at the substations are modeled as dispatchable loads, curtailable at a very large price compared to the generation cost. Therefore, the objective of the problem in this study is to minimize the unmet demand in the network.

The third step is to simulate the performance of the power network by cutting off the failed transmission lines determined by the simulations introduced in Section 6. As a result of this removal, some parts of the power network may form sub-grids. In each sub-grid, a check is performed first to determine if there are any generators. If the sub-grid does not contain any generators, then all the power demand of the sub-grid is assumed to be unmet. If at least one generator exists in the sub-grid, then the number of busses in the sub-grid is considered. If there is only one bus, then there is no need to run the ACOPF model, since the demand and supply can be calculated directly. If there are more than one buses, a slack bus will be assigned to one of the generators and the model runs an ACOPF to determine the power redistribution among the buses. The simulation stops when all sub-grids achieve a stable power flow and the demand unserved for the whole network is computed and stored. If the analyses cannot reach convergence, load-shedding is performed to shed 5% load in the area with overflowed branches. This load-shedding is repeated until convergence of the optimal power flow is achieved. If the convergence has not been achieved after 20 load-shedding steps, the system is deemed to be collapsed and the overflowed branches are removed. This method captures the branch overflow, bus load shedding, and branch failures and is able to model cascading failures in the power network. More details on the simulation procedure can be found in the literature [23].

The above simulation procedure is repeated for the 4000 network transmission line failure samples obtained in Section 6. Each samples consists of 13 time steps reflecting the network configuration throughout the duration of the hurricane event. Therefore, the total number of power flow simulation is 52,000. At each buses, the expected power loss (demand not served) can be computed as follows:

$$EDS_j(t) = \frac{\sum_{n=1}^{N_I} \sum_{t=1}^{N_T} DS_j(n,t)}{N_I} \tag{16}$$

where $DS_j(n,t)$ is the demand not served at bus j in sample n at time step t, $N_T = 13$ is the total number of time steps , $N_I = 4000$ is the total number of samples. Fig. 26 shows the expected unmet demand for all 67 distribution substations during the hurricane. It can be seen that the distribution substations in the network suffer quite different power losses. Six distribution substations in close proximity are predicted to suffer expected unmet demand larger than 90 MWh. The households in the area served by these substations are expected to have very high risk of outage under the simulated hurricane. With such knowledge, proactive measures can be taken to provide backup power sources for the critical buildings in those areas. In general, the substations that are far from the hurricane track are expected to suffer by lower amounts of unmet demand, which is consistent with the simulation results of the transmission line failure probability shown in Fig. 23.

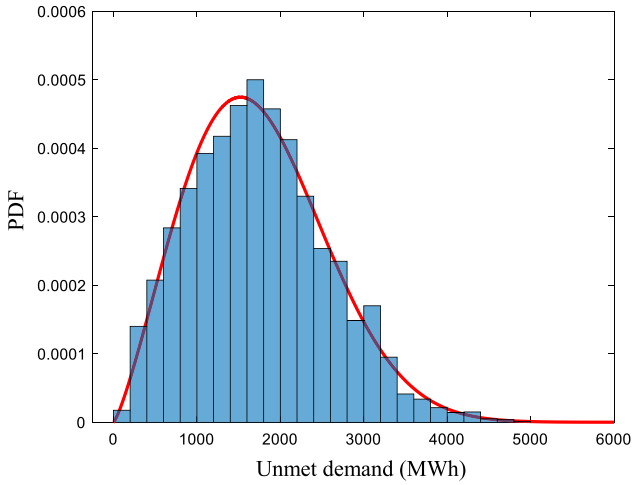

Fig. 27. PDF of the power network unmet demand.

Fig. 27 shows the histogram of the total unmet demand of the power network. The probability density histogram of the unmet demand can be well fitted by a Weibull distribution. The two parameters Weibull distribution is formulated as:

$$f(x|a,b) = \begin{cases} \frac{a}{b}(\frac{x}{b})^{a-1} e^{-(\frac{x}{b})^a} & x \geq 0 \\ 0 & x < 0 \end{cases} \tag{17}$$

with $a = 2.2612$ and $b = 1969.7$. The mean of the power network unmet demand is 1744 MWh. Simulation results of the hourly unmet demand for the power network are shown in Fig. 28. The load curtailment is most likely to happen at t_6 and t_7 when the power network is experiencing the most unfavorable wind field. In most cases, the hourly unmet demand remain unchanged after t_9, since the most unfavorable wind condition for the network has passed, and there is little chance of transmission line failure afterwards. It is noted that the hourly unmet demand curve may decrease during the event. The reason is that the connections between some power plants and the substations outside of

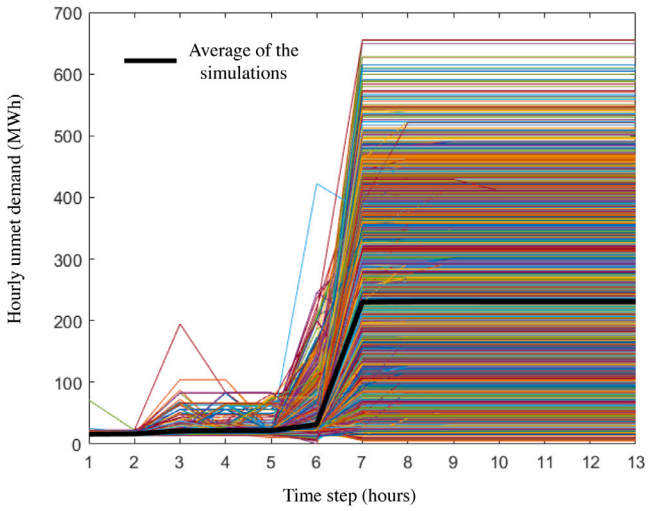

Fig. 28. Simulation results of hourly unmet demand; each line in the plot represents one simulation result of the network.

Table 7
Comparison of four methods under investigation.

	Proposed method	Method 1	Method 2	Method 3
Time-varying effects	✓			✓
Wind direction	✓	✓		✓
Correlation	✓	✓	✓	

the Lehigh Valley region may be lost, and therefore more power become available for the Lehigh Valley region.

The simulation results not only serve as an assessment of the power network performance but reveal the weakness of the power network. According to the simulation results, suggestions can be provided to the power network operators and mangers to optimize the performance of the power network. For instance, deployment of the portable power generation at the buses predicted to suffer the most load curtailment before the hurricane arrives can significantly reduce the unmet demand in the power network. From a long-term perspective, an upgrade of the vulnerable transmission lines as shown in Fig. 23 can reduce the failure probability of these transmission lines and increase the resilience of the power system.

The proposed methodology is compared to three simplified methods as described in Table 7. For Method 1, only the maximum wind intensity and its corresponding wind direction are used to perform transmission line failure simulation, so that no structural component failure happens before the maximum wind intensity is reached. Method 2 computes the transmission line failure probability without taking the time-varying effects and the wind direction into consideration. It assumes that the structures are subjected to the most unfavorable wind attack angle. This method is commonly used because the hurricane wind direction field is difficult to obtain. Method 3 assumes that all structures behave independently without any correlation, therefore all the values of the random field discussed in Section 5 are computed independently. Fig. 29 shows the probability density function of the unmet demand computed by the proposed method and the three other methods mentioned above. Table 8 shows the average, maximum and minimum value of the unmet demand computed by the proposed methods and the three simplified methods. It can be seen that Method 1 and Method 3 result in less unmet demand than the proposed method. Method 2, which only takes the wind intensity into consideration, results in the largest unmet demand. As shown in Table 8, ignoring the time-varying effects and correlation might be acceptable for a quick evaluation of the system performance. However, in order to develop a rigorous assessment of the power network performance, it is necessary to consider the effects of the wind direction, correlation among structural failures and time-varying failure probability of the structures.

Table 8
Simulation results of the four methods under investigation.

	Proposed method	Method 1	Method 2	Method 3
Average unmet demand (MWh)	1744.6	1624.6	3622.0	1694.6
Maximum unmet demand (MWh)	4891.3	4679.6	7209.7	4749.6
Minimum unmet demand (MWh)	153.0	79.4	229.3	149.4

8. Conclusions

In this paper, a novel framework for the probabilistic simulation of the power transmission network performance under hurricanes was presented. A synthetic but very close to reality power network model was developed, with details of the electrical and structural characteristics based on a campaign of image processing and data mining. A hurricane simulator was utilized to obtain details on a specific hurricane event with significant impact on the study region. Failures of two types of structures (i.e., transmission towers and conductors) are considered in this study using physics-based fragility models. Fragility pools are created to properly incorporate the time-varying effects and uncertainties in the structural capacity into the simulation of the transmission lines failure. This study quantifies the power system performance through ACOPF analysis and investigates the importance of time-varying and wind direction effects.

One of the most important challenges in this research was to develop a method that could make the fragility models compatible with the time-varying probability of failure assessment. To the best of the author's knowledge, all current methodologies have just ignored the uncertainty in the capacity to make the fragility model compatible. To address this challenge, a novel procedure was developed to deaggregate the uncertainties in load and capacity from the fragility models. Fragility pools were generated to allow implementation of the fragility models without having to ignore the uncertainties in capacity. Results from the analysis indicate that the transmission towers are much more vulnerable than the conductors, and the transmission line failures are mostly due to the failures of the transmission towers. However, for some transmission lines with some relatively long conductor spans under unfavorable winds, the conductor failure is not negligible and should be properly accounted for. The results of the system performance computed by four methods are compared in the study. The main finding of this comparison is that the time-varying effects, wind direction and correlation among structures all have impact on the system performance. However, wind direction has the largest impact on the system performance; ignoring this factor will result in significant overestimation of the unmet demand in the system.

There are some limitations to the applicability of the proposed method, which could be addressed in the future research. First, the method is scenario-based. Therefore, to assess the power system performance unconditional to a specific hurricane, a large amount of hurricane samples are needed. Generating these samples and conducting analyses requires huge computational power and/or time. To this respect, advanced optimal scenario sampling techniques need to be developed in order to address this limitation. Second, the recovery of the power system after the hurricane is not part of the scope of this research. However, recovery is a critical factor, which affects the system performance. The community will suffer much less from the unmet demand if the infrastructure has a speedy recovery. Future studies are needed for the simulation of the restoration process of the power transmission systems.

The proposed method serves as a tool for regional power network quantitative risk and resilience assessment. It can effectively evaluate

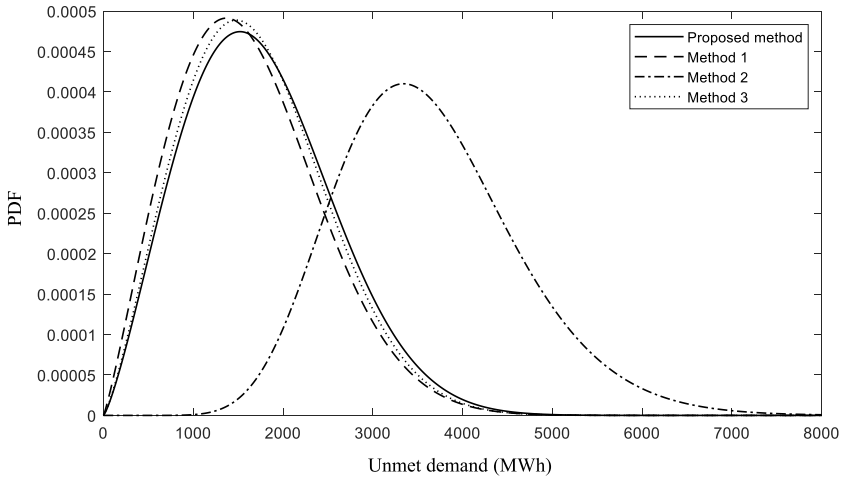

Fig. 29. PDF of the power network unmet demand.

the power transmission network performance under hurricanes over time and space. In the short-term perspective, the technique can be utilized to identify the vulnerable parts of the system under a specific hurricane, and therefore help utility companies to take proactive measures, such as deployment of portable power generation, to effectively mitigate the impact of an approaching hurricane. In the long-term perspective, the simulation results based on the proposed method can be used by decision makers to optimize the retrofitting strategy of the system, such as planning upgrades of the weakest transmission lines to enhance the system resilience.

CRediT authorship contribution statement

Liyang Ma: Conceptualization, Methodology, Software, Visualization, Validation, Writing – original draft. **Vasileios Christou:** Software, Methodology, Writing – review & editing. **Paolo Bocchini:** Supervision, Conceptualization, Resources, Funding acquisition, Writing – review & editing.

Declaration of competing interest

The authors declare that they have no known competing financial interests or personal relationships that could have appeared to influence the work reported in this paper.

Acknowledgments

This work is part of the "Probabilistic Resilience Assessment of Interdependent Systems (PRAISys)" project (www.praisys.org). The support from the National Science Foundation, USA through grant CMMI-1541177 and from the Pennsylvania Department of Community & Economic Development, USA through grant PIT-19-02 is gratefully acknowledged.

The authors would like to acknowledge also Dr. Wenjuan Sun (Lehigh University), Akanksha Dubey (National Grid) and Chase Gallik (Wiss, Janney, Elstner Associates, Inc.) for their contributions during the development of this research project.

The opinions and conclusions presented in this paper are those of the authors and do not necessarily reflect the views of the sponsoring organizations.

References

[1] Sun W, Bocchini P, Davison BD. Policy-based disaster recovery planning model for interdependent infrastructure systems under uncertainty. Struct Infrastruct Eng 2020;17:555–78.
[2] Sharma N, Nocera F, Gardoni P. Classification and mathematical modeling of infrastructure interdependencies. Sustain Resilient Infrastruct 2020;1–22.
[3] Sharma N, Tabandeh A, Gardoni P. Regional resilience analysis: A multiscale approach to optimize the resilience of interdependent infrastructure. Comput-Aided Civ Infrastruct Eng 2020;35:1315–30.
[4] Shinozuka M, Dong X, Chen T, Jin X. Seismic performance of electric transmission network under component failures. Earthq Eng Struct Dyn 2007;36:227–44.
[5] Zhang H, Cheng L, Yao S, Zhao T, Wang P. Spatial–temporal reliability and damage assessment of transmission networks under hurricanes. IEEE Trans Smart Grid 2019;11:1044–54.
[6] Hurricane harvey event analysis report. North American Electric Reliability Corporation; 2018.
[7] Hoffman P, Bryan W. Comparing the impacts of northeast hurricanes on energy infrastructure. Technical report, Office of Electricity Delivery and Energy Reliability; 2013.
[8] Fu X, Li H-N, Tian L, Wang J, Cheng H. Fragility analysis of transmission line subjected to wind loading. J Perform Constr Facil 2019;33:04019044.
[9] Fu X, Li H-N, Li G. Fragility analysis and estimation of collapse status for transmission tower subjected to wind and rain loads. Struct Saf 2016;58:1–10.
[10] Mohammadi Darestani Y, Wang Z, Shafieezadeh A. Wind reliability of transmission line models using kriging-based methods. In: 13th international conference on applications of statistics and probability in civil engineering(icasp13). 2019.
[11] Fu X, Li H-N. Uncertainty analysis of the strength capacity and failure path for a transmission tower under a wind load. J Wind Eng Ind Aerodyn 2018;173:147–55.
[12] Xiao F, McCalley JD, Ou Y, Adams J, Myers S. Contingency probability estimation using weather and geographical data for on-line security assessment. In: 2006 international conference on probabilistic methods applied to power systems. IEEE; 2006, p. 1–7.
[13] Ma L, Bocchini P, Christou V. Fragility models of electrical conductors in power transmission networks subjected to hurricanes. Struct Saf 2020;82:101890.
[14] FEMA. HazUS-MH 4.2 hurricane model technical manual. 2018.
[15] Winkler J, Duenas-Osorio L, Stein R, Subramanian D. Performance assessment of topologically diverse power systems subjected to hurricane events. Reliab Eng Syst Saf 2010;95:323–36.
[16] Ouyang M, Duenas-Osorio L. Multi-dimensional hurricane resilience assessment of electric power systems. Struct Saf 2014;48:15–24.
[17] Zio E, Golea LR. Analyzing the topological, electrical and reliability characteristics of a power transmission system for identifying its critical elements. Reliab Eng Syst Saf 2012;101:67–74.
[18] Xue J, Mohammadi F, Li X, Sahraei-Ardakani M, Ou G, Pu Z. Impact of transmission tower-line interaction to the bulk power system during hurricane. Reliab Eng Syst Saf 2020;203:107079.
[19] Song J, Cotilla-Sanchez E, Ghanavati G, Hines PD. Dynamic modeling of cascading failure in power systems. IEEE Trans Power Syst 2015;31:2085–95.
[20] Li J, Shi C, Chen C, Dueñas-Osorio L. A cascading failure model based on ac optimal power flow: Case study. Physica A 2018;508:313–23.
[21] Mei S, Ni Y, Wang G, Wu S. A study of self-organized criticality of power system under cascading failures based on ac-opf with voltage stability margin. IEEE Trans Power Syst 2008;23:1719–26.

[22] Vaiman M, Bell K, Chen Y, Chowdhury B, Dobson I, Hines P, Papic M, Miller S, Zhang P. Risk assessment of cascading outages: Methodologies and challenges. IEEE Trans Power Syst 2012;27:631.
[23] Li J, Dueñas-Osorio L, Chen C, Shi C. Ac power flow importance measures considering multi-element failures. Reliab Eng Syst Saf 2017;160:89–97.
[24] Birchfield AB, Gegner KM, Xu T, Shetye KS, Overbye TJ. Statistical considerations in the creation of realistic synthetic power grids for geomagnetic disturbance studies. IEEE Trans Power Syst 2016;32:1502–10.
[25] Christou V. Advanced simulation of uncertain quantities in civil engineering with applications to regional hazards (Ph.D. thesis), Lehigh Univeristy; 2019.
[26] US Census Bureau. Population, housing units, area, and density: 2010 - county – census tract. 2010, URL: https://factfinder.census.gov/faces/tableservices/jsf/pages/productview.xhtml?src=CF.
[27] Exelon Generation. Limerick generating station. 2018, URL: http://www.exeloncorp.com/locations/power-plants/limerick-generating-station (Retrieved from date 17 June 2018).
[28] Talen Energy. Susquehanna nuclear power plant. 2018, URL: http://susquehannanuclear.com (Retrieved from date 17 June 2018).
[29] Exelon Generation. Limerick generating station. 2018, URL: http://www.exeloncorp.com/locations/power-plants/three-mile-isl{and} (Retrieved from date 17 June 2018).
[30] Calpine. Bethlehem energy center. 2018, URL: http://www.calpine.com/pennsylvania/bethlehem-energy-center (Retrieved from date 17 June 2018).
[31] NRG Energy. Gilbert power station. 2018, URL: http://maps.nrg.com/media/attachments/PLA.2015_Gilbert_v4HR.pdf (Retrieved from date 17 June 2018).
[32] Talen Energy. Gilbert power station. 2018, URL: https://www.talenenergy.com/generation/fossil-fuels/martins-creek (Retrieved from date 17 June 2018).
[33] Dyegy Inc. Ontelaunee energy facility. 2018, URL: https://www.dynegy.com/locations (Retrieved from date 17 June 2018).
[34] US Energy Information Administration. Levelized cost and levelized avoided cost of new generation. 2020, URL: https://www.eia.gov/outlooks/aeo/pdf/electricity_generation.pdf.
[35] US Energy Information Administration. Table 6.7.a. capacity factors for utility scale generators primarily using fossil fuels. 2020, URL: https://www.eia.gov/electricity/monthly/epm_table_grapher.php?t=epmt_6_07_a.
[36] Vickery PJ, Wadhera D. Statistical models of holland pressure profile parameter and radius to maximum winds of hurricanes from flight-level pressure and h* wind data. J Appl Meteorol Climatol 2008;47:2497–517.
[37] Vickery PJ, Wadhera D, Powell MD, Chen Y. A hurricane boundary layer and wind field model for use in engineering applications. J Appl Meteorol Climatol 2009;48:381–405.
[38] Zhang JA, Uhlhorn EW. Hurricane sea surface inflow angle and an observation-based parametric model. Mon Weather Rev 2012;140:3587–605.
[39] ASCE. Design of lattice steel transmission structures. 2015, http://dx.doi.org/10.1061/9780784413760.
[40] Gaylord EH, Wilhoite GM. Transmission towers: Design of cold-formed angles. J Struct Eng 1985;111:1810–25.
[41] Ma L, Khazaali M, Bocchini P. Component-based fragility analysis of transmission towers subjected to hurricane wind load. Eng Struct 2021;242:112586.
[42] Ma L, Christou V, Bocchini P. Probabilistic simulation of power transmission systems affected by hurricane events based on fragility and ac power flow analyses. In: 13th international conference on applications of statistics and probability in civil engineering(icasp13). 2019.
[43] Farzaneh M, Savadjiev K. Evaluation of tensile strength of acsr conductors based on test data for individual strands. IEEE Trans Power Deliv 2006;22:627–33.
[44] Bocchini P, Frangopol DM, Deodatis G. A random field based technique for the efficiency enhancement of bridge network life-cycle analysis under uncertainty. Eng Struct 2011;33:3208–17.
[45] Bocchini P, Frangopol DM. A stochastic computational framework for the joint transportation network fragility analysis and traffic flow distribution under extreme events. Probab Eng Mech 2011;26:182–93.
[46] Marelli S, Sudret B. Uqlab: A framework for uncertainty quantification in matlab. In: Vulnerability, uncertainty, and risk: quantification, mitigation, and management. 2014, p. 2554–63.
[47] Zimmerman RD, Murillo-Sánchez CE, Thomas RJ. Matpower: Steady-state operations, planning, and analysis tools for power systems research and education. IEEE Trans Power Syst 2010;26:12–9.